BBA - Bioenergetics 1860 (2019) 148053

Contents lists available at ScienceDirect

BBA - Bioenergetics

journal homepage: www.elsevier.com/locate/bbabio

Pigment-protein complexes are organized into stable microdomains in cyanobacterial thylakoids

A. Strašková[1], G. Steinbach[1,2], G. Konert, E. Kotabová, J. Komenda, M. Tichý, R. Kaňa*

Institute of Microbiology, Czech Academy of Sciences, Centre Algatech, Novohradská 237, 379 81 Třeboň, Czech Republic

ARTICLE INFO

Keywords:
Photosynthesis
Confocal microscopy
Photosystems
Thylakoid membrane
Membrane heterogeneity
Microdomains
Cyanobacteria
Population heterogeneity

ABSTRACT

Thylakoids are the place of the light-photosynthetic reactions. To gain maximal efficiency, these reactions are conditional to proper pigment-pigment and protein-protein interactions. In higher plants thylakoids, the interactions lead to a lateral asymmetry in localization of protein complexes (i.e. granal/stromal thylakoids) that have been defined as a domain-like structures characteristic by different biochemical composition and function (Albertsson P-Å. 2001,Trends Plant Science 6: 349–354). We explored this complex organization of thylakoid pigment-proteins at single cell level in the cyanobacterium *Synechocystis* sp. PCC 6803. Our 3D confocal images captured heterogeneous distribution of all main photosynthetic pigment-protein complexes (PPCs), Photosystem I (fluorescently tagged by YFP), Photosystem II and Phycobilisomes. The acquired images depicted cyanobacterial thylakoid membrane as a stable, mosaic-like structure formed by microdomains (MDs). These microcompartments are of sub-micrometer in sizes (~0.5–1.5 μm), typical by particular PPCs ratios and importantly without full segregation of observed complexes. The most prevailing MD is represented by MD with high Photosystem I content which allows also partial separation of Photosystems like in higher plants thylakoids. We assume that MDs stability (in minutes) provides optimal conditions for efficient excitation/electron transfer. The cyanobacterial MDs thus define thylakoid membrane organization as a system controlled by co-localization of three main PPCs leading to formation of thylakoid membrane mosaic. This organization might represent evolutional and functional precursor for the granal/stromal spatial heterogeneity in photosystems that is typical for higher plant thylakoids.

1. Introduction

Biological membranes were originally described as a fluid mosaic with uniform distribution of proteins and lipids [1]. Later, heterogeneous membrane areas were found in a form of lipid rafts in animal cells [2], various bacterial microdomains (MDs) [3–5] or raft-like MDs in mitochondria [6]; it led to a change in the paradigm of membrane organization proposing mosaic macrostructure of cellular membranes with specific MDs [7]. Recently, a heterogeneous distribution of membrane proteins has been intensively discussed also in plant cytoplasmic membranes [8,9] or in plant mitochondrial membrane [10]. The mitochondrial enzymes of oxidative phosphorylation (OXPHOS) are known to form heterogeneous membrane compartments [11–13] that highly restrict the diffusion of OXPHOS enzymes [14]. Therefore, a "plasticity model" of inner mitochondria membranes has been suggested [15].

Chloroplast represents other bioenergetics organelle of higher plants and algae. Light-photosynthetic reactions proceed on thylakoid membrane that is heterogeneously structured into stacked and unstacked regions defined as granal and stromal thylakoids (see e.g. the most recent reviews [16–18]). Grana are stabilized by physicochemical forces [19,20] controlled by ion compartmentation [21]. All primary photochemical reactions, including light-harvesting, charge separation and subsequent electron transport processes are catalyzed by heterogeneously distributed membrane proteins complexes of Photosystem I (PSI), Photosystem II (PSII) and cytochrome b_6f complex. There is a clear lateral asymmetry between granal/stromal thylakoids that form (micro)domains with different biochemical composition and function [22]. Typically, a higher PSII/PSI ratio is typical for granal (stacked) and lower for stromal (unstacked) thylakoids [22]. In higher plants, the light-harvesting efficiency of photosystems is increased by their membrane embedded pigment-protein antennas of photosystems (e.g.

* Corresponding author.
E-mail address: kana@alga.cz (R. Kaňa).
[1] A. Strašková and G. Steinbach contributed equally to this study.
[2] Present address: Institute of Biophysics, Biological Research Center, Szeged, Hungary.

https://doi.org/10.1016/j.bbabio.2019.07.008
Received 5 December 2018; Received in revised form 28 June 2019; Accepted 18 July 2019
Available online 22 July 2019
0005-2728/

LHCII).

It contrasts with cyanobacteria in which the light-harvesting antenna complexes, Phycobilisomes (PBS) [23] are situated on the thylakoid membrane surface and can form huge functional megacomplexes with both photosystems [24]. In fact, cyanobacteria represent an evolutionary ancestor of plant chloroplasts [25,26]. Their thylakoids harbor components of respiratory electron transport chain [27] and their thylakoids show no signs of the membrane stacking [28,29]. This makes cyanobacteria a unique model system to study localization of thylakoid protein complexes independently of membrane stacking. *In vivo* microscopic data have suggested a heterogeneous distribution of pigment-protein complexes (PPCsincluding PSI, PSII and PBS) in thylakoids of various cyanobacterial strains including *Synechocystis sp.*, *Synechococcus* sp. or *Anabaena* sp. Based on these data, several distinct models of PPCs organization in cyanobacterial thylakoids were built proposing either radial (i.e. with variability between inner/outer thylakoid layers [30–32]) or lateral [33,34] heterogeneity in PPCs, especially photosystems, composition. Different methods used in these studies also led to different conclusions in respect to the photosystems location: PSI has been preferentially localized either to the outermost (see electron microscopic data in [32]) or to the inner membrane thylakoids (see hyperspectral confocal fluorescence image data in [31]). Moreover, *in vitro* AFM experiments with isolated thylakoid membrane proposed existence of a specific type of small PSI MDs in *Synechocystis* sp.PCC 6803 [35]; electron microscopy pictures showed arrays of PSII in the same organism [36]; a specific bioenergetics MDs were recognized by confocal microscopy in *Gloeobacter violaceus* [37], a primitive thylakoid-less cyanobacterium [38]. These results clearly showed non-existence of a conclusive model for the thylakoid membrane organization of PPCs in cyanobacteria.

In the present work we addressed complex organization of thylakoid membrane proteins by a simultaneous *in vivo* detection of all major PPCs (PSI, PSII, PBS) by means of 3D confocal imaging. Our data proved heterogeneous organization of these PPCs into microdomains (MDs) that define mosaic like structure of thylakoid membrane of *Synechocystis* sp. PCC 6803 strain. This conclusion is based on following methods and results: (1) Simultaneous three channel localization of PPCs [39] has been adapted for 3D imaging of the whole cyanobacterial thylakoid; (2) YFP tagging of PSI [40] allowed localization of PSI in 3D structure of cyanobacterial thylakoid; (3) The new method of image processing (segmentation) defined/quantified seven possible types of thylakoid membrane MDs; (4) Each MD was typical by particular PPCs ratios and microdomains did not segregated PPCs from each other; (5) Only three most dominant MDs were found in the most cells, namely (a) PSI dominant MD; (b) PSI & PSII & PBS MD; (c) PSII & PBS dominant MD; (6) The 3D organization of MDs showed mosaic-like organization of the cyanobacterial thylakoids; (7) MDs are of sub-micrometer in size (~0.5–1.5 μm); (8) MDs are very stable in a range of several minutes as shown by FRAP and time-lapse imaging. We suggest that the observed MDs stability is conditional for efficient excitation/electron transfer. In conclusion, our structural model of cyanobacterial thylakoid membranes is based on localization of all three PPCs (PSI, PSII, PBS), that interact together and synergistically form the thylakoid membrane mosaic. The mosaic distribution pattern of MDs in the cyanobacterial thylakoids reminds of the distinct location pattern of PSII and PSI in granal/stromal thylakoids of higher plant chloroplasts [22] and might represent its evolutionary precursor.

2. Methods

2.1. Growth of cells and strain generation

The YFP tagged strain used in the study was derived from the GT-P variant of the glucose-tolerant strain of *Synechocystis* sp. PCC 6803 [41] (hereafter referred to as *Synechocystis* 6803) previously described in [42] and hereafter referred to as WT. To generate a strain expressing PsaF-YFP fusion at the C-terminus of PsaF, pUC18:*psaF*-YFP-Cm^R plasmid was used to transform the *Synechocystis* WT strain as described in [40]. This plasmid was constructed by insertion of the YFP coding sequence (corresponding to a Venus sequence, [43]) at the end of the 3′ coding region of the *psaF* gene (*sll0819*). As a selectable marker chloramphenicol-resistance gene (Cm^R) was inserted downstream of the *psaJ* (*sml0008*) gene which is located downstream the *psaF* gene in the *Synechocystis* genome. Transformants were selected on BG11 plates with 5 μg/mL chloramphenicol, genome copies were segregated by plating on the chloramphenicol concentration up to 40 μg/mL. PCR was used to show integration of YFP and elimination of the WT gene copies. The strains were cultivated on a rotary shaker under moderate light conditions (white light, 40 μmol of photons $m^{-2} s^{-1}$, 30 °C) in liquid BG11 medium.

Accession Numbers: Sequence data from this article can be found in the GenBank/EMBL databases under the following accession numbers: PsaF (Sll0819), BAA18108; and PsaJ (Sml0008).

2.2. Analysis of protein complexes

Thylakoid membranes were prepared by breaking cells with zirkonia/silica beads using Mini-Beadbeater (BioSpec Products, USA) as described by [44]. The protein composition of cyanobacterial membranes was analyzed by two-dimensional polyacrylamide gel electrophoresis (PAGE) combining clear native electrophoresis (CN-PAGE) with denaturing SDS-PAGE. CN-PAGE was performed in 4–14% gradient polyacrylamide gel (acrylamide to BIS-acrylamide ratio was 1:60) according to [45] with modifications described in [46]. Native gels were photographed and scanned for chlorophyll fluorescence. Individual proteins in membrane complexes separated by CN-PAGE were resolved in the second dimension by SDS-PAGE in a denaturing 12–20% linear gradient polyacrylamide gel containing 7 M urea. Separated proteins were further visualized by staining with Coomassie Blue (Quick Coomassie Stain; Generon, Ltd., GB) and the identity of the stained PSI proteins was verified by mass spectrometry as described in [47].

2.3. Measurements of PSI activity

PSI activity was determined from P700 oxidation and re-reduction kinetics using a Dual-PAM-100 (Walz, Germany) in the dual-wavelength mode $\Delta(I_{875}\text{-}I_{830})$. Complete P700 oxidation was induced by a 30 ms saturation pulse (I = 10,000 μmol photons $m^{-2} s^{-1}$). Steady state (P), maximal (Pm, Pm′) and zero (Po) P700 levels were determined at defined actinic light intensities stepwise-increasing (logarithmic increment) from 0 to 825 μmol photons $m^{-2} s^{-1}$ with 30 s adaptation periods. Quantum yield of photochemical energy conversion at PSI [Y(I) = 1-Y(ND)-Y(NA)] and quantum yields of non-photochemical energy dissipation due to donor side limitation [Y(ND) = 1-P700red.] and due to acceptor side limitation [Y(NA) = (Pm-Pm′)/Pm] were calculated by Dual-PAM software according to [48].

2.4. Measurement of PSII variable fluorescence

The maximum quantum yield of PS II photochemistry (F_V/F_M) and effective PSII antennas size (σPSII) were detected by fast repetition rate fluorescence (FRRF) method [49] by custom-designed FL3500 fluorometer (Photon Systems Instruments, Brno, Czech Republic) at 28 °C with dark-adapted samples (10 min). Single-turnover flashes were induced by application of a series of 120 of sub-saturating flashlets (1.5 μs duration) either blue (λ = 463 nm) reflecting PSII antennas size due to chlorophyll absorption, or amber (λ = 590 nm) light reflecting PSII antennas size of PBS. The single turnover flash was fitted according to the model of Kolber and co-workers [49] giving the σPSII. Fv/Fm was calculated as $(F_M\text{-}F_o)/Fm$ (F_M and F_o - the maximum and minimum fluorescence in dark adapted state).

2.5. Oxygen evolution, chlorophyll concentrations and absorption spectra

Oxygen evolution normalized to the chlorophyll a content was measured at 28 °C using a Clark-type DW2/2 electrode chamber (Hansatech, United Kingdom) in the presence of 5 mM sodium bicarbonate. The rate of gross oxygen evolution was calculated from the slope of net O_2 evolution measured at saturating irradiance 500 μmol photons $m^{-2} s^{-1}$ (KL1500, SCHOTT, USA) plus the slope of respiratory O_2 uptake measured in the dark just after light exposure.

Chlorophyll a content was estimated by extraction from cell pellets with 100% (v/v) methanol at room temperature using Thermo Spectronic Helios Epsilon spectrophotometer according to Porra and co-workers [50].

–

2.6. Confocal microscopy

2.6.1. Image acquisition

Confocal images were acquired by Leica SP8 microscope (Leica Microsystems Inc. Wetzlar, Germany) equipped with SuperK EXTREME white laser source (NKT Photonics A/S, Birkerød, Denmark) and a HC-PL-APO CS2-63x/1.4 oil immersion objective. The measuring protocol contained 2 repeated *Z*-stack scans (with 225 nm step in z) to address a possible effect of image fading. The optical slices (in Z direction) were optimized by a confocal pinhole adjustment to 1 AU, a 64 × 64 pix (pixel size 60 nm, 48× zoom) pictures were imaged in x-y. The 3 channel RGB pictures were collected in 2 scans: (1) simultaneous detection of YFP signal (Ex: 488 nm; Em: 500–550 nm, detected by Leica Hybrid Detector, gain 150%), chlorophyll autofluorescence (Ex: 488 nm; Em: 690–790 nm, detected by Leica Hybrid Detector, gain 130%) and transmission images (at 633 nm, transmission PMT detector, gain 319 V); and (2) phycobilisomes autofluorescence (Ex: 633 nm, Em: 645–680 nm, fluorescence PMT detector, gain: 682 V) measurements. The two laser lines were provided by the white laser source, 488 nm at 3% intensity, 633 nm at 0.03% intensity.

2.6.2. Image processing, construction 3D image

Images were exported by the Leica software to standard 24 bit TIFF format and later post processed by ImageJ macros [51] as merged multipage RGB TIFF images. A possible fading caused by *Z*-stack measurement was corrected for each channel independently by two successive *Z*-stacks of the same cell. The averaged fading parameter was calculated for the three RGB channel separately (Red channel – f_R, Green channel – f_G; Blue channel – f_B) from fading detected between two successive Z-stacks in particular image in the stack as $f_i = \sqrt[k]{I_i/I_{i+k}}$ (k – total number of the slices in z-stacks; i – image position in the single stack) using an ImageJ macro determining changes in the individual fluorescence intensities (I_i and I_{i+k}) between 2 subsequent *Z*-stacks measurements. The average fading parameters for RGB channels (f_R = 1.006; f_G = 0.989; f_B = 1.002 for single scans) were then applied to all images in the 1st stack as a constant correction factor. The raw Z-stack images were processed by ZEN Black software (version 2.1, Carl Zeiss Microscopy GmbH, Germany) to be displayed in 3D. The transparency mode was used (Threshold 13%, Ramp 50%, Maximum 100%) with spatial parameter for X-Y = 0.06 μm & Z – 0.225 μm respectively (view angle 45°).

2.6.3. Image processing – RGB image segmentation into microdomains

The RGB images were segmented based on the relative fluorescence intensity in three detected channels (intensity of PSII fluorescence in red channel – I_R, intensity of PSI-YFP fluorescence in Green channel – I_G, intensity of PBS fluorescence in blue channel – I_B). The RGB cube was divided into 8 volumes (7 representing the MDs and one for background, see Supplemental Fig. 3) when the black background (i.e. pixels having intensity lower than 100 on the 8-bit scale for all three channels) was excluded from the segmentation.

The segmentation algorithm compares the relative intensity of the channels pixel-by-pixel (see Supplemental Fig. 3D). If one from the three channels (I_R, I_G or I_B) is higher by a factor of 1.15 (≫) than the remaining two, then the corresponding color (red/green/blue) is selected. When the relative intensity of two channels ($I_R \wedge I_G$, $I_R \wedge I_B$ or $I_B \wedge I_G$) is similar (~, i.e. the fluorescence ratio is in a range (1/1.15; 1.15)), but higher by a factor of 1.15 (≫) than the third channel, yellow, magenta or cyan is selected respectively. The ratio 1/1.15 was selected after testing all other approximate values and recognized as the most optimal for the used microscopic setup; it means the output of segmentation (i.e. thresholder binary pictures in 7 colors) co-localized with original colors of RGB pictures as defined by *colorimetric standards* CIE 1931 for human vision [52]. This algorithm resulted in 7 combinations, that allowed us to segment RGB pixels into 7 different groups that determined basic MDs with characteristic intensity & color combinations: (1) Red MD, dominant in PSII ➔ $I_R \gg [I_B \wedge I_G]$ (2) Green MD – dominant in PSI ➔ $I_G \gg [I_B \wedge I_R]$; (3) Blue MD – dominant in PBS ➔ $I_B \gg [I_G \wedge I_R]$; (4) Yellow MD – dominant in PSI & PSII ➔ $[I_G \sim I_R] \gg I_B$; (5) Cyan MD – dominant in PSI & PBS ➔ $[I_G \sim I_B] \gg I_R$; (6) Magenta MD – dominant in PSII & PBS ➔ $[I_R \sim I_B] \gg I_G$; (7) white/grey MD with a "*similar*" (~) intensity in all channels $I_R \sim I_B \sim I_G$. The volume of particular MD in the RGB cube-color space reflects number of possible pixel color combinations (I_R, I_B and I_G) in particular MD (see Supplemental Fig. 3). The algorithm counting the amount of pixels having different color-combinations was analysed for every cell containing several *Z*-stack images separately, and the data were used for calculations from all cells.

2.6.4. Image post-processing, 3D visualization

The three dominant MDs present in segmented images were visualized in 3D using PovRay software (Persistence of Vision Raytracer Pty. Ltd. Williamstown, Victoria, Australia, http://povray.org/). Every pixel of the three most abundant areas (green – PSI, white/grey – PSI-PSII-PBS and magenta – PSII-PBS) was represented by an ellipsoid with diameters: 60 nm, 60 nm, 225 nm according to the slice/pixel size for the 3D model. During the reconstruction process the elementary ellipsoids were transformed into a *blob-object* and finally rendered by Persistence of Vision Raytracer program.

2.6.5. Characterization of pixel distribution in RGB color space

The overall distribution of PSI, PSII and PBS in cells was calculated from RGB images. The intensities of red, green and blue channels (I_R, I_G, I_B) in every pixel were characterized by the RGB values transformed into two coordinate of CIE 1931 color space [53] by ImageJ [51]. The more detailed application of RGB color space for data processing of 3 channel images of photosynthetic microdomains has been presented by Konert and co-workers [54]. The total distribution of the fluorophores in PSI-YFP cells was represented in 3D plot.

2.6.6. Fluorescence Recovery After Photobleaching (FRAP) measurements

Mobility measurements of PSI (based on YFP fluorescence) and PSII (based on chlorophyll autofluorescence) was carried out with a laser-scanning confocal microscope (Zeiss LCM 880, Carl Zeiss Microscopy GmbH, Germany) equipped with a Zeiss Plan-Apochromat 63× oil objective (NA = 1.4). The YFP and chlorophyll fluorescence was excited by Argon Laser laser (488 nm laser line), fluorescence was detected in two channel mode simultaneously, in the 690–735 nm/530–560 nm spectral ranges for chlorophyll/YFP fluorescence respectively. The imaging was done with following parameters: zoom: 20×; pinhole: 64 μm; pixel dwell time: 4.12 μs; sequential imaging: 1 fps framerate at 128 px × 128 px; dichroic mirror: MBS 488/543/633. Bleaching was induced during 500 ms when the bleached area was set-up to be 500 nm × 500 nm; it resulted in the bleach depth of 50%. The exported raw data files were processed by Visual Basic macros (Microsoft Excel 2010, Microsoft Corp.).

Table 1
Proportional percent representation of individual photosynthetic microdomains in thylakoid membrane of *Synechocystis* 6803 PSI-YFP. The values were calculated together for all cells, values represent means ± s.d. from all images acquired during *Z*-stack scanning (n = 200) when all the images were analyzed together as averaged for all cells. The meta-analysis of the whole cell population, with calculation of MDs presence/absence per single cell is presented in 3 including their statistical analysis. The bold values represents values for three most dominant MDs, see Fig. 4.

Microdomains	PSI	PSI-PSII-PBS	PSII-PBS	PSII	PSI-PSII	PBS	PSI-PBS
Color	Green	White/grey	Magenta	Red	Yellow	Blue	Cyan
	52.5 ± 28.0	**21.3 ± 13.0**	**10.0 ± 15.7**	6.0 ± 13.1	6.2 ± 6.8	2.8 ± 7.0	1.2 ± 2.9

2.6.7. Analysis of distribution of microdomains in cell population

Distribution of MD count in every cell was explored using RGB images after segmentation (see Section 2.6.3). Every cell was analyzed separately (number of cells: 39, full *Z*-stack containing between 8 and 12 images) and the distribution of MD count per single cell in the cell population was plotted (value 1 - homogeneous cell, value 7 - maximally heterogeneous cell). The calculation employed the process of segmentation (see Section 2.6.3), when each thylakoid membrane pixel was assigned to one of 7 possible types of MDs (Red, Green, Blue, Magenta, Cyan, Yellow, White marked as R, G, B, M, C, Y and W, respectively). First, MD size in particular cell was calculated as a percentage of total thylakoid area by ImageJ macro (see Section 2.6.3) and presented for all cells together as an average MD size per whole cell population (Table 1), the number of MDs in every cells from population was then plotted separately (Fig. 3). During calculation of MD occurrence in cell population, only MDs with the sizes equal or higher than 10% were included in the summary. This threshold (10%) for MD size was imposed as it reflected an average size of MDs that covers at least 10% of thylakoid membrane area.

2.6.8. Statistical test on significance of MDs distribution in cell population

We have statistically tested if the observed occurrence of 3 largest domains in the cell population is of statistical significance in comparison to their random distribution. First, we have calculated the theoretical probability of every possible combination of three largest MDs to appear in the cell. This included also cells containing only one or two MDs that fulfilled requirements of covering more than 10% thylakoid area (see definition in Section 2.6.7). The expected random distribution of MDs in cells population was then compared with observed distribution based on the analysis of total MDs occurrence in the cell population (see Section 2.6.7. from Materials and methods). In details, the theoretical random distribution (all possible types of cells) included all possible combination was calculated based on combinatorics equation:

$$N = \frac{md!}{k!(md-k)!}$$

where N represented total theoretical combinations of MDs (N), md – all possible types of MDs (i.e. R, G, B, M, C, W in total md = 7) and k stands for count of MDs in a theoretical cell (1, 2 or 3) as written in Supplemental Table 1. Based on k value, there were three theoretical groups: Group I - cells with only one type of MDs (i.e. homogeneous cells), combinations of 1 element (k = 1) from md = 7; Group II - cells with two types of MDs (two colors), combination of 2 elements (k = 2) from md = 7; Group III - cells with 3 types of MDs (three colors), combinations of 3 element (k = 3) from md = 7. The sum of these three equations resulted in total 63 possible theoretical MD combinations (7, 21 and 35 for group I, II and III respectively). This number represented the theoretical random distribution of MDs with no special preference, and every possible MDs combination (see Supplemental Table 1) had a theoretical probability to occur 1/63 = 1.587%. Statistically, the expected frequencies between each of 63 possible top 3 MDs compositions were 1:1.

Further, we have evaluated if the observed frequencies of MDs based on experimental data (Supplemental Table 1) differed significantly in comparison to the expected theoretical proportions (Supplemental Table 1) by application of *G*-test [55] implemented in R-software (version 3.4.4, GNU license). We have tested whether the occurrence of cells containing only variations of MDs composed from G, W, M or their combinations (see yellow marked combinations in Supplemental Table 1) was present statistically more often than random MDs distribution in cell population. The theoretical expected count of MDs combinations composed of G, W, and M in population (i.e. statistically their frequency) was 7 (G, W, M, GW, GM, MW, GWM, see Supplemental Table 1). The expected frequencies were converted to account the size of the cell population sample we measured (n = 39); it resulted in frequencies expected 0.62 per every combination of MD. The observed number of cells falling into specific top 3 MD categories composed of G, W, M in the all three groups (I, II and III) were counted to be 30 (Supplemental Table 1) that was used as an input for *G*-test in R software.

3. Results

3.1. Strain generation and their photosynthetic parameters

The organization of major PPCs in thylakoid membranes in vivo was studied in a *Synechocystis* 6803 strain expressing the Venus variant of yellow fluorescent protein (YFP) on C terminus of the PsaF subunit (PSI-YFP strain [40]. This modification of PsaF resulted in the formation of PSI complexes tagged at the cytoplasmic side of the thylakoid membrane (Fig. 1A). The presence of YFP-tagged PSI complexes was confirmed by analysis of membrane protein complexes by clear native (CN) and SDS polyacrylamide gel electrophoresis (2D-CN/SDS PAGE) [46]. Both WT and PSI-YFP showed a similar pattern of PSI and PSII complexes (Supplemental Fig. 1, 1D scan and 1D fluorescence) in the CN gel, the only difference represented by low abundance additional green band with mobility similar to the PSII monomer that lacked both PsaF and PsaF-YFP (see SDS page in Supplemental Fig. 1). Importantly, SDS PAGE (Supplemental Fig. 1) confirmed substitution of PsaF in the PSI-related bands in the in YFP-PSI strain, by a larger PsaF-YFP protein as it has been previously identified [40].

The basic physiological parameters (growth rate or pigment composition) were not affected in the PSI-YFP cells and PSI/PSII ratio is not changed in the *Synechocystis* sp. PCC 6803 expressing the fluorescently tagged PSI [40]. We further characterized the photosynthetic parameters of this strain (Fig. 1). We have proved no effect of YFP tagging on PSII activity; the rate of oxygen evolution and maximal efficiency of PSII photochemistry also remained unaffected (Fig. 1B). The YFP tagging did not affect either PSII connectivity (see legend of Fig. 1) or the effective chlorophyll antenna size of PSII (see σ_{PSII} for blue excitation in Fig. 1B). Importantly, the YFP tagging, even though YFP sticks out of the membrane by about 4 nm (see the scheme in the Fig. 1A), its presence does not affect interaction of Phycobilisomes (PBS) with PSII as shown in unchanged σ_{PSII} for excitation to phycobilins (see σ_{PSII} for amber excitation, Fig. 1D). Similarly, YFP tagging did not affect PSI photochemistry, either in its P_{700} oxidation–reduction kinetics (Fig. 1C, upper panel), or in the light-dependency of steady-state values of quantum yields of PSI photochemical energy conversion [Y(I)] and non-photochemical energy dissipation [Y(NA)] (Fig. 1C, lower panel). As

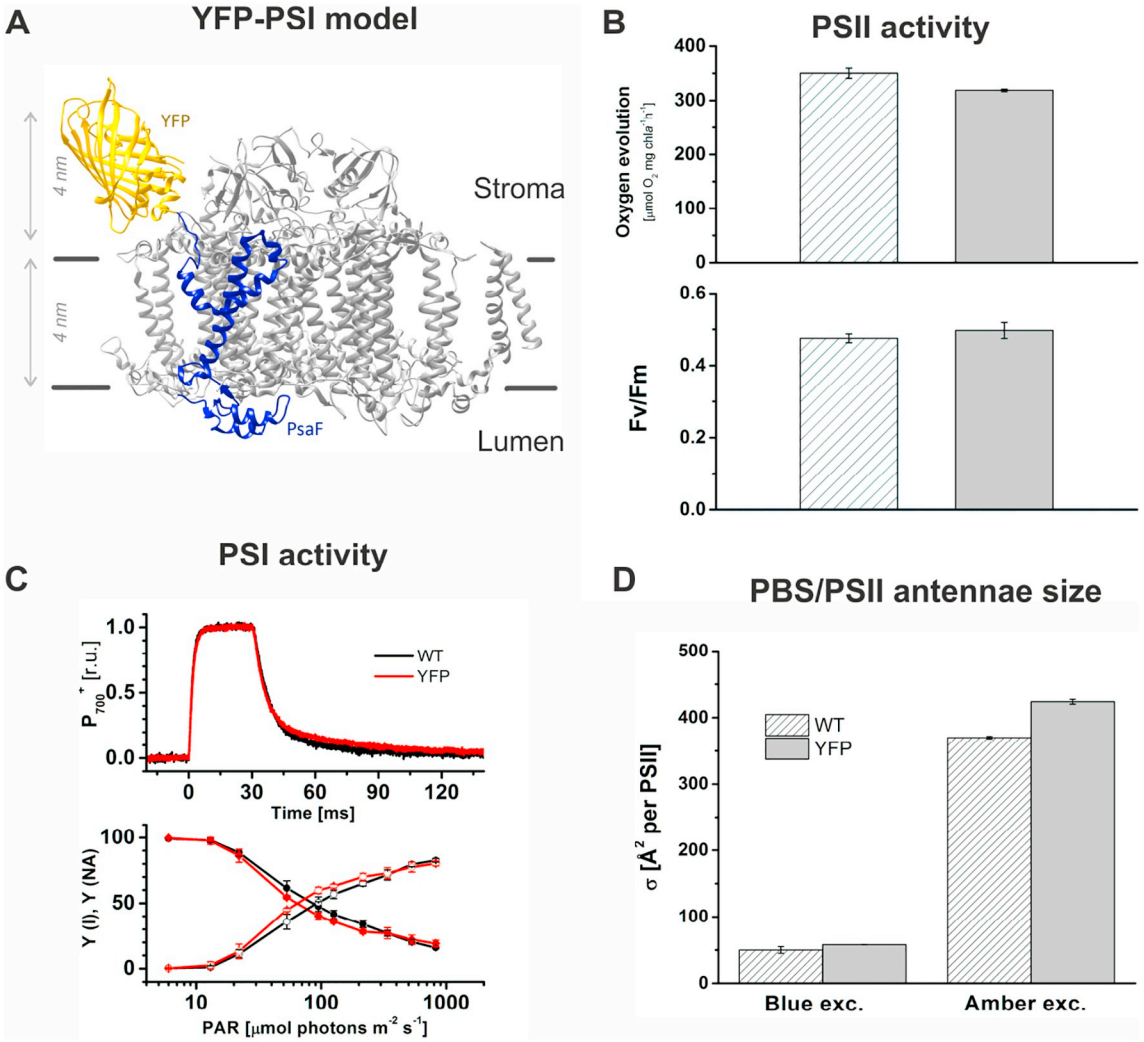

Fig. 1. Basic physiological characteristics of the PSI-YFP *Synechocystis* 6803 strain. (**A**) The structural model of cyanobacterial PSI monomer with YFP (in yellow) attached to the C-terminus of the PsaF subunit (in blue) and exposed to the cytoplasm, the averaged width of thylakoid membrane bilayer (4 nm) and YFP protein are marked; (**B**) Photochemical properties of PSII in WT (hatched bar) and PSI-YFP mutant (grey bar) cells characterized by measurement of gross oxygen evolution (upper graph) and maximum quantum yield of PSII photochemistry (Fv/Fm). (**C**) Photochemical properties of PSI characterized by measurement of P700 oxidation and reduction kinetics (P_{700}^{+}) and quantum yield of photochemical energy conversion and non-photochemical energy dissipation in WT (black) and PSI-YFP mutant cells (red). Quantum yield of photochemical energy conversion in PSI [Y(I); closed symbols] and quantum yield of non-photochemical energy dissipation due to acceptor side limitation [Y(NA); open symbols] were derived from steady state (P), maximal (Pm, Pm′) and minimal (Po) P700 levels at defined light intensities during rapid light curves with 30 s adaptation periods at stepwise-increased (logarithmic increment) actinic light intensities from 0 to 825 μmol photons·m^{-2}·s^{-1}. No donor side limitation was detected [Y(ND) ≈ 0]. (**D**) Measurement of chlorophyll (blue excitation) and phycobilisome (amber excitation) effective antenna size of PSII (σ) in WT (hatched bar) and in PSI-YFP cells (grey bar). The blue excitation wavelength was 463 nm and the amber excitation wavelength was 590 nm. The connectivity of PSII reaction centers was $p = 0.373 \pm 0.007$ in WT and 0.410 ± 0.001 in PSI-YFP mutant (blue excitation at 463 nm). All datasets above represent mean ± s.d. of three biological replicates. Organization of photosynthetic protein complexes in WT and in PSI-YFP strains (clear native SDS-PAGE) are presented in the supplemental Fig. 1.

the YFP did not affect either PSI/PSII photochemistry or PBS attachment to PSII, it makes the PSI-YFP strain ideal model to the study organization of all PPCs in vivo.

3.2. Presence of specific thylakoid membrane microdomains in *Synechocystis* 6803

The native organization of PPCs, namely PSI, PSII and PBS, in thylakoid membrane was addressed by 3 channel confocal microscopy based on detection of PSII (red channel) and PBS (blue channel) autofluorescence simultaneously with YFP fluorescence of PSI (green channel) (Supplemental Fig. 2). The setup allowed us to describe localization of the most important thylakoid membrane proteins thus providing us a good proxy for the overall organization of thylakoid proteins. The RGB images of the PSI-YFP cells acquired in the middle cell layer (Fig. 2A) reflected spatial organization and ratios of individual PPCs inside thylakoid membranes (Fig. 2). These membrane PPCs were found to be organized into special microcompartments characterized by their RGB color (see RGB color coding description in Fig. 2). The presence of heterogeneous microcompartments in RGB was detectable independently of confocal microscopy setup (data not shown). In our typical setup (see Materials and Methods), the acquired images (Fig. 2) showed three dominant colors occurring decreasingly in the following order: green (see e.g. cell C1), white/grey (see e.g. A5) and magenta (see e.g. A4). The rest of the basic RGB color combinations were almost absent (e.g. red) or visible in a few specific cells (see e.g. cell C3 for yellow; cell C6 for cyan and blue, cell C3 for yellow in Fig. 2A). The three dominant combinations of PPCs were repeatedly

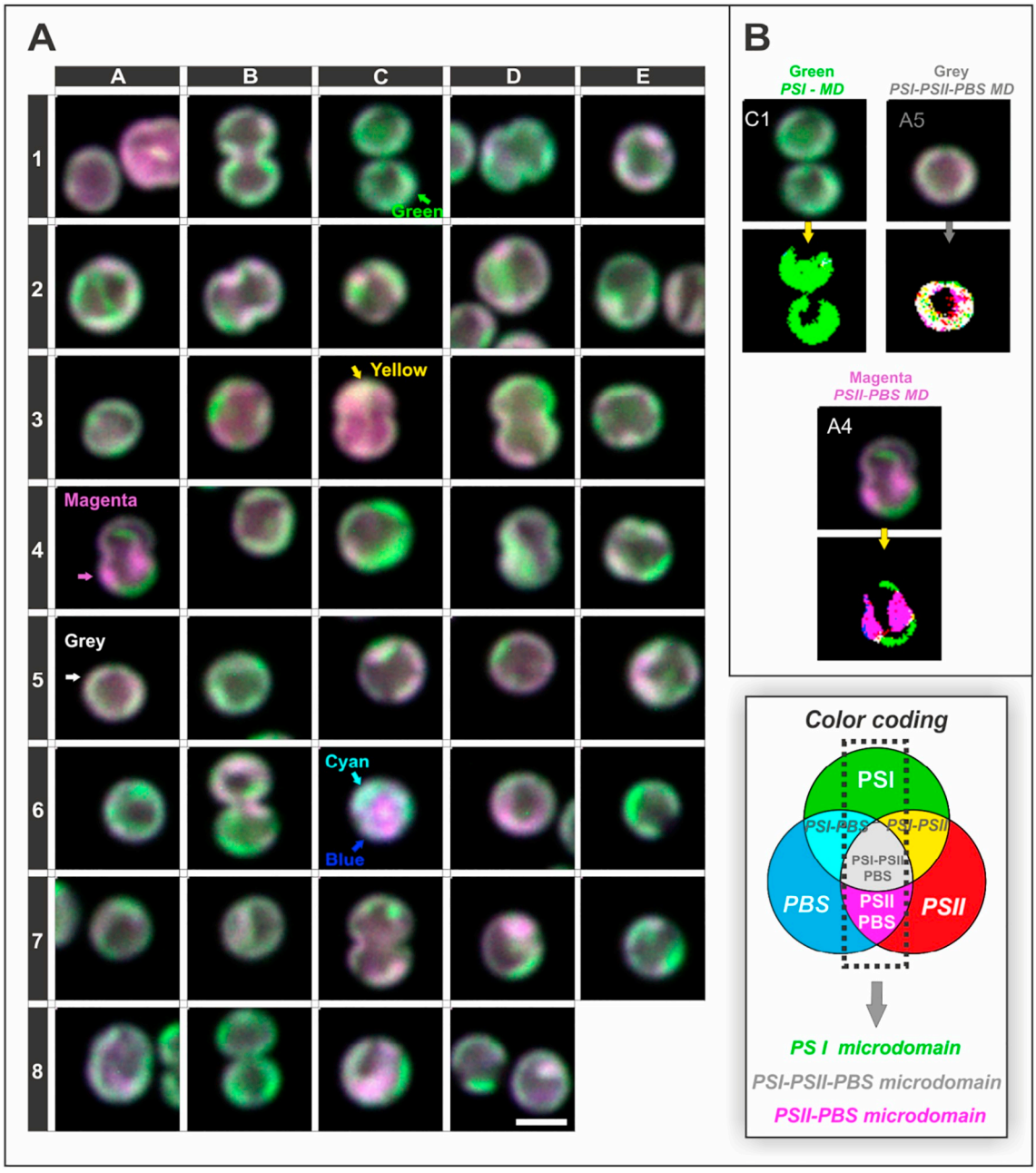

Fig. 2. RGB image of thylakoid membrane microdomains formed by three pigment-protein complexes (Photosystem I, Photosystem II and Phycobilisome) and microdomain segmentations. (**A**) The RGB picture represents three independently acquired channels, autofluorescence of Photosystem II (PSII, in red) and Phycobilisome (PBS, blue) together with YFP fluorescence of Photosystem I (PSI in green) (see Supplemental Fig. 2 for separate channels in greyscale). All possible combinations of three measured channels are represented by RGB color space with 7 basic combinations as described in the scheme: (1) Red color – dominant PSII emission; (2) Green color – dominant PSI emission; (3) Blue – dominant PBS emission; (4) Yellow – dominant PSI & PSII emissions with minimal PBS autofluorescence; (5) Magenta – dominant PSII & PBS emissions with minimal YFP fluorescence from PSI, (6) Cyan – dominant PSI & PBS emissions with minimal PSII autofluorescence; (7) White/Grey – similar PSI, PSII PBS emissions. The combined image shows typical cross section of 39 independently measured cells representing one layer of the *Z*-stack scan of the whole cell. Scale bar 2 μm. (**B**) RGB image segmentation into different microdomains. The image represents binary RGB image after application of segmentation method (see Materials and Methods, Supplemental Fig. 3 and 4) that defines characteristic areas of MD as defined in the enclosed scheme.

visible in different cells in a form of specific microcompartments with hundreds nanometers in size (Fig. 2). Even though these areas were variable in their shape/position inside of thylakoid, they always kept similar colors. Based on the qualitative analysis of pictures we have proposed that these 3 microcompartments represent a specific photosynthetic MDs, that are defined by their RGB color, it means by the specific combinations of PSI(YFP)/PSII/PBS fluorescence intensity. Based on definition of RGB color space, magenta MD represents areas with dominant PSII & PBS emissions (much smaller YFP emission from PSI), green MD is characteristic by dominant YFP emission of PSI (and smaller PSII and PBS fluorescence) and white/grey was typical by balanced of PSII, PBS and YFP-mediated PSI emissions.

3.3. Microdomains quantification in thylakoid membrane and their cell-to-cell heterogeneity

We quantified abundancy of photosynthetic MDs by a newly developed method of RGB image segmentation (see Materials and Methods, and Supplemental Fig. 3 and Supplemental Fig. 4) and by statistical meta-analysis of whole cell population (see Materials and Methods, and Fig. 3, Supplemental table 1). The calculation of the average MD composition calculated for all cells together confirmed the dominance of the green PSI-MD, magenta PSII-PBS MD and white/grey PSI-PSII-PBS MD (Table 1). These three most dominant MDs covered more than 80% of thylakoid membrane area calculated as average from all cells. However, the bulk-type of analysis (i.e. MD areas were averaged per all cells together) covered the hidden population heterogeneity clearly visible between cells (Fig. 2). Indeed, except green, magenta and white, also the other colors (red, yellow, blue, cyan in Fig. 2) were occasionally present in few specific cells (see e.g. C3 for yellow; cell C6 for cyan and blue as seen in the Fig. 2).

Therefore, we also calculated the typical combination of MD areas per single cells (Fig. 3). First, we have estimated the most common number of MDs per cell (Fig. 3) and later we also calculated the typical MD composition per cell (see Supplemental Table 1). In both cases, the most frequent number of the dominant MDs was three, and 80% of cells were heterogeneous (Fig. 3) with most dominant combination of MDs represented by green PSI-MD, magenta PSII-PBS MD and white/grey PSI-PSII-PBS MD. This was confirmed by both the averaged RGB image segmentation (Table 1) and the meta-analysis cell-by-cell for whole population (see Supplemental Table 1 and Fig. 3). Further, we also statistically tested a significance of the three dominant MDs in single cell (green, magenta, white) by *G*-test (see Materials and methods, Supplemental Table 1). Indeed, the analysis proved that the observed most frequent MD combination in the population of cells significantly differed from MD combinations that assume the equal probability of their occurrence (see Supplemental Table 1).

We subsequently analyzed the three dominant MDs in more details (Fig. 4). In contrast to recently described seemingly homogenous small MDs of PSI observed in isolated thylakoids of *Synechocystis* 6803 in vitro [35] we found that in our MDs the major photosynthetic complexes are not strictly segregated. So, the magenta PSII-PBS MDs always exhibited a weak signal of YFP reflecting the presence of small amount of PSI in this MD (Fig. 4A), nevertheless the signal of PSII (red) and PBS (blue) fluorescence was almost doubled in comparison with the YFP fluorescence of PSI (see e.g. peripheral part of the cell profile in the Fig. 4B). The white/grey MDs were typical by an approximately equal presence of all three PPCs, which was reflected by their balanced fluorescence emissions (see histogram/profiles in Fig. 4D and E) while in the green MDs the YFP emission of PSI exceeded almost twice the emission of PSII and PBS documenting the dominance of PSI over PSII and PBS in this MD (see fluorescence histogram/profile in Fig. 4G and H). Thus, the photosynthetic MDs with specific PSI/PSII/PBS ratios define a mosaic like structure of thylakoid membrane.

3.4. 3D model of thylakoid microdomains distribution and microdomains stability

The mosaic like distribution of MDs within the thylakoids has been further characterized by different Z sectioning and 3D reconstruction of thylakoid membrane system in *Synechocystis* 6803 (see Fig. 5 for workflow). Size of photosynthetic MDs (particularly green and magenta) were not completely uniform (between 0.5 and 1.5 μm) and they were often separated by sharp edges (see Fig. 5C, see e.g. the enclosed Movie 5). The white/grey MDs were often situated in between the other two most dominant MDs in the most typical cyanobacterial cells (see MDs variability in Fig. 3). This is shown in our model of thylakoid membrane (Fig. 5D) based on the *Z*-stack images (Supplemental Fig. 6A, Supplemental Fig. 7A), which shows organization of PPCs into

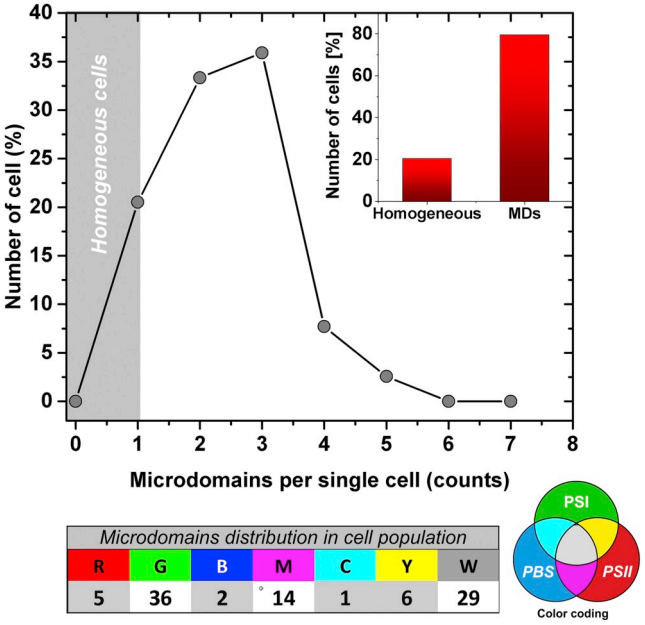

Fig. 3. Distribution of number of microdomain counts per single cell in the studied population of *Synechocystis* sp. *PCC 6803 cells*. The figure characterizes distribution of microdomain counts per single cell in the population of cyanobacteria. The value "1" represents homogeneous cell with single type of MD, values in the range "2" to "7" reflect heterogoneous cells with various number of MDs (see Supplemental Table 1 for details). The MDs counts in single cell have been calculated from 3D cell image after image segmentation (see Section 2.6.3) when only membrane areas with the size equal or higher than 10% were counted as MDs (see Section 2.6.7). Insert shows number of homogeneous/heterogeneous cells. The bottom table shows total number of particular MDs in cell populations (counted cell by cell) where R, G, B, M, C, Y and W mean Red, Green, Blue, Magenta, Cyan, Yellow, and White/Grey MDs respectively. Total number of cells used for analysis was 39. The microdomains combinations presented in the analysis are based on 3 channel confocal fluorescence measurement (PSI (YFP) fluorescence – green; PSII fluorescence – red; PBS fluorescence – blue). The resulted RGB color pictures can contain 7 possible types of MDs (see insert of Color coding): (1) Red color – MD with dominant PSII emission; (2) Green color – MD with dominant PSI emission; (3) Blue – MD with dominant PBS emission; (4) Yellow – MD with dominant PSI & PSII emissions and minimal PBS autofluorescence; (5) Magenta – MD with dominant PSII & PBS emissions with minimal YFP fluorescence from PSI; (6) Cyan – MD with dominant PSI & PBS emissions with minimal PSII autofluorescence; (7) White/Grey – MD with similar PSI, PSII, and PBS emissions. For further details, see Supplementary Table 1.

mosaic from different angles (Supplemental Fig. 6A, Supplemental Fig. 7A, Movie 6 and Movie 7). The 3D model reflects a separation of PPCs into the magenta PSII-PBS MDs surrounded by white/grey PSI-PSII-PBS MDs and more distantly by green PSI MDs. As the white/grey intermediate PSI-PSII-PBS MD exhibits the balanced fluorescence of all three PPCs (Fig. 4D), it was not so visible in the single layer RGB image (Fig. 3) also due to a limited spatial resolution of confocal microscopy.

We also tested a stability of MDs using a time-lapse imaging together with **F**luorescence **A**fter **P**hotobleaching **R**ecovery (FRAP) method (Fig. 6). The two channel detection allowed us to address PSI and PSII mobility simultaneously (Fig. 6). A comparison of "*Pre-bleach*" ($t = 0$ s), "*After-bleach*" ($t = 6$ s) and "*Recovery*" ($t = 300$ s after bleaching period) for chlorophylls (reflecting localization of PSII) and YFP (reflecting localization of PSI) showed no change in organization of MDs and overall mosaic like structure of thylakoids during 6 min of image acquisition (Fig. 6A) also including the bleaching period (see cyan arrow in Fig. 6A). Moreover, the MDs outside of bleach area with high abundancy of PSI (see green arrows in Fig. 6A) and PSII (see red arrows in Fig. 6A) were also stable during image acquisition on a scale

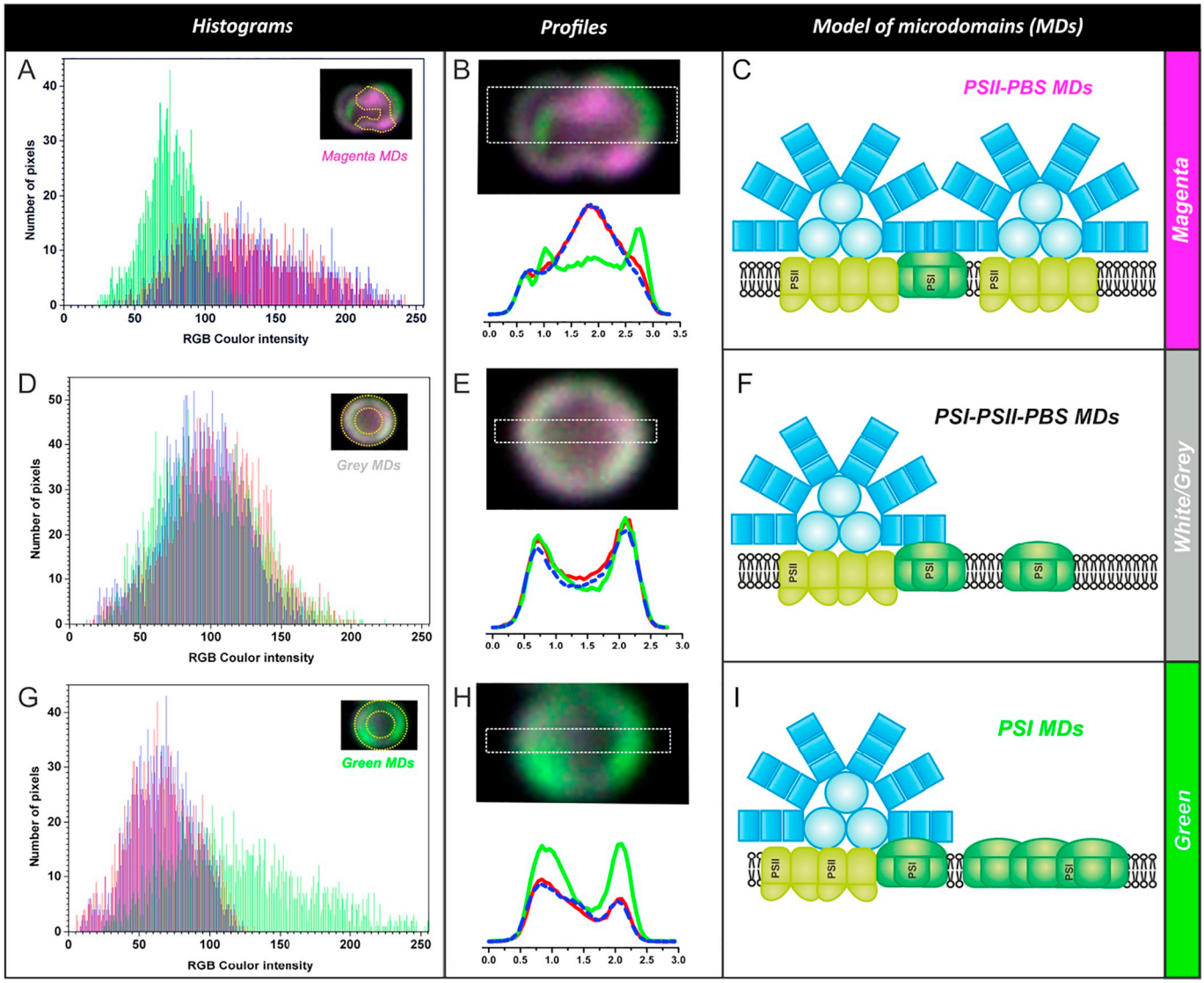

Fig. 4. Proposed pigment-protein composition of photosynthetic microdomains (MDs) based on fluorescence intensities. The model shows proposed pigment-protein complexes composition in three dominant microdomains (magenta – PSII-PBS MDs; white/grey – PSI-PSII-PBS MDs; green – PS MDs) that reflects Photosystem I (PSI), Photosystem II (PSII) and Phycobilisomes (PBS) content and distribution in MDs. The model is based on fluorescence characteristics of MDs represented by histograms and fluorescence profiles of selected cells. The three fluorescence intensities detected by confocal microscope are drawn in their characteristic colors for red channel (chlorophyll emission from PSII), green channel (YFP emission from PSI) and blue channel (phycobilin emission from PBS).
Model and fluorescence characteristics of **magenta MD**, i.e. PSII-PBS MD: (**A**) Typical fluorescence histograms in PSII-PBS MD; (**B**) Profiles of fluorescence intensity in selected cell in PSII-PBS MD; (**C**) Simplified model of PSII-PBS MD.
Model and fluorescence characteristics of **grey/white MD**, i.e. PSI-PSII-PBS MD: (**D**) Typical fluorescence histograms of PSI-PSII-PBS MD; (**E**) Profiles of fluorescence intensity in selected cell in PSI-PSII-PBS MD; (**F**) Simplified model of PSI-PSII-PBS MD.
Model and fluorescence characteristics of **green MD**, i.e. PSI MD: (**G**) Typical fluorescence histograms of PSI MD; (**H**) Profiles of fluorescence intensity in selected cell in PSI MD; (**I**) Simplified model of PSI-PSII-PBS MD. Data represent typical histograms from magenta, green and white/grey areas visible in Fig. 2.

of minutes. The FRAP measurement also allowed us a detailed assessment of the PSII and PSI mobility in the membranes (see Fig. 6B). The data were in line with the previously shown (see e.g. review [56]) low mobility of PSI and PSII in cyanobacteria (see Fig. 6B). Such a low mobility clearly explains the stable mosaics like organization of PPCs within the thylakoid membrane of *Synechocystis 6803* (Fig. 5).

4. Discussion

There have been several attempt to study thylakoid membrane heterogeneity in cyanobacteria by various in vitro methods including proteomics [57], electron microscopy [28,32,36], AFM microscopy [35] or cryo-imaging [34]. Based on the confocal microscopy approach, MacGregor-Chatwin and coworkers [35] has shown heterogeneity of PSI, however there were no quantitative analysis details about PSI co-localization with PSII and PBS and no 3D model of PSI occurrence. Further, in the work of Casella and co-workers [33] authors have discussed and shown 2D co-localization of PSI + PSII, however PBS were again not detected and none from the picture were quantified by image segmentation. Finally, in the Vermaas's work [31] authors did indeed address all the three main channels PPCs, however the occurrence was judged from spectra deconvolution by hyperspectral confocal fluorescence method without any fluorescence tagging. We used a different, more native approach. It is based on a combination of fluorescence tagging of protein complexes and life imaging of cyanobacterial cells by confocal microscope. Interestingly, we came with different conclusion in contrast to work [31] as we did not see radial but rather lateral heterogeneity in PPCs. Further, we have also seen no segregated

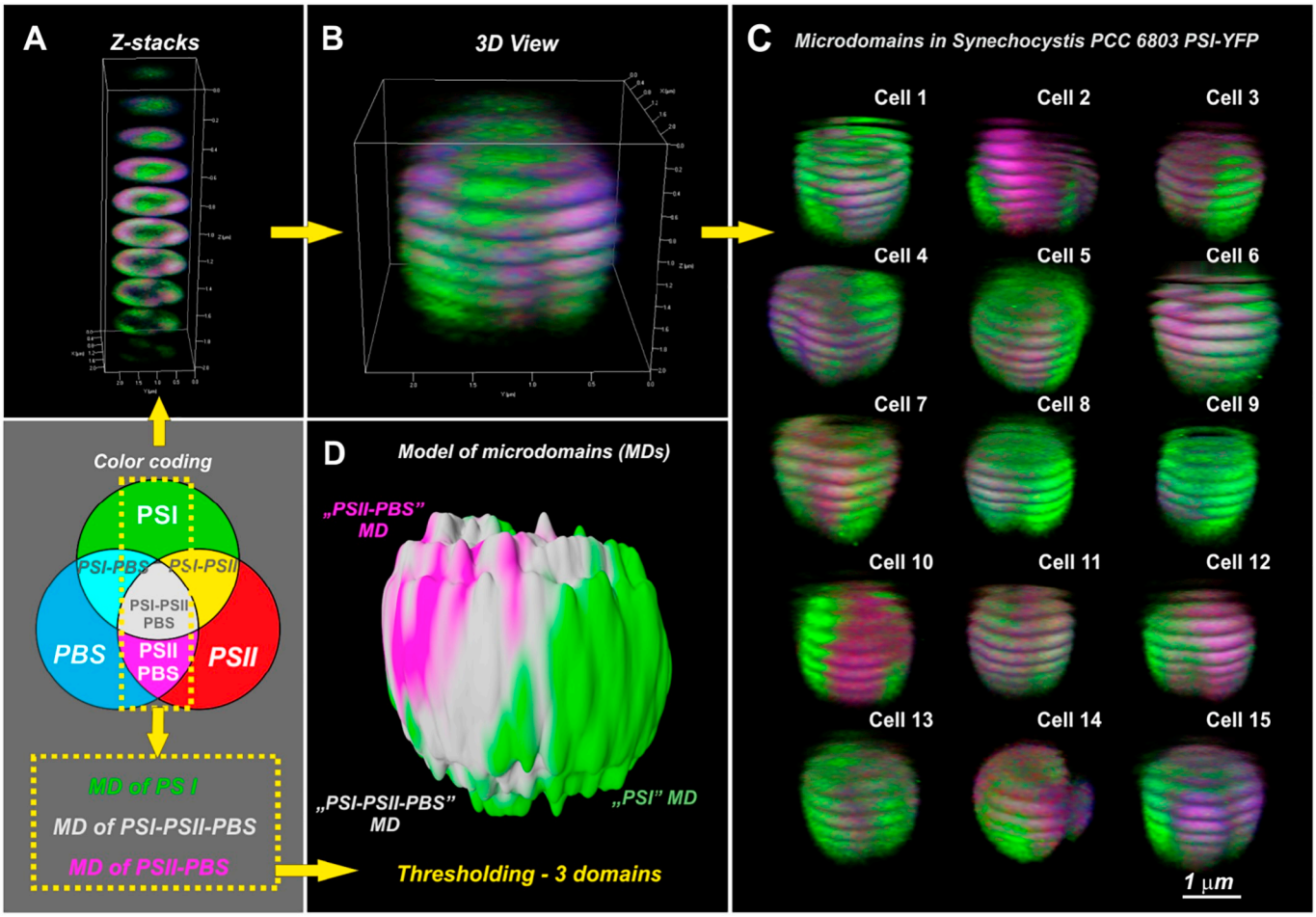

Fig. 5. Thylakoid membrane mosaic of photosynthetic microdomains (MDs) based on 3D images in *Synechocystis* 6803 PSI-YFP cells. MDs are formed by pigment-protein complexes of Photosystem I (green), Photosystem II (red) and Phycobilisome (blue) but only 3 of the 7 possible combinations are dominant (see yellow rectangle): (1) Green MD (with prevailing PSI abundancy); (2) white/grey MD (balanced PSI–PSII–PBS content); (3) Magenta MD (prevailing PSII-PBS abundancy); (4) cyan (prevailing PSI–PBS abundancy); (5) yellow (prevailing PSI–PSII abundancy); (6) blue (prevailing PBS abundancy); (7) red (prevailing PSII abundancy). (**A**) Z-stack images of a single cell (see Movie 1); (**B**), A reconstituted 3D Z-stack of single cell from Panel A, a distance between section was 0.225 µm; (**C**), MDs structure and organization in different cells constructed based on Z-stack images (Supplemental Fig. 5, Movies 2, 3, 4 for cells 1–3); (**D**) A 3D model of MDs, constructed from cell no. 6 (see Supplemental Fig. 6 for workflow and Movie 6), based on segmented data (see example in Supplemental Fig. 4).

microdomains of PSI in vivo in contrast to conclusion of MacGregor and co-workers [35]. Based on our data, PSI complex in thylakoid membrane is every time inter-mix with PSII, with different PSI/PSII ratio in different MDs (e.g. PSI content is very high in green MD, see Fig. 4).

We suggests that thylakoid membrane organization can be consider as a specific system of 3 PPCs that works together and form thylakoid membrane mosaic (see Fig. 5). In fact, there is only a limited combination in PPCs as we have described recently by new photosynthetic parameter called Protein arrangement factor (see Supplemental Fig. 8 and [54]). The authors proved that even during long-term irradiation, the fluorescence ratios of PSI/PSII/PBS (defining MDs structure) did not change on average on cell population level [54]. Our new approach presented here allowed us to further identify the internal heterogeneous organization of thylakoid membrane as a complex system defined by three PPCs. We describe cyanobacterial thylakoid membrane as a mosaic structure consisting of stable photosynthetic MDs (Fig. 5) typical by specific ratio of three major PPCs: PSI, PSII and PBS (Fig. 4). In addition, we performed the meta-analysis of data cell-by-cell and this also confirmed the presence of several MDs in a single cyanobacterial cell (Fig. 3). We have analyzed number of MDs per single cell, the analysis proved that only 20% cells were relatively homogenous (see insert in Fig. 3) and the remaining cells were heterogeneous with MDs. These cells had usually three major types of MDs represented by magenta MD (dominant PSII & PBS emissions), green MD (dominant YFP emission of PSI) and white/grey MD (balanced PSII, PBS and YFP-PSI emissions). This represents the most common type of MDs organization that we further discuss in our model (Fig. 7). MDs organization was different only in some specific cells (see e.g. cell C3 for yellow; cell C6 for cyan and blue, cell C3 for yellow in Fig. 2) and this can be easily explained by the observed population heterogeneity (see Supplemental Table 1 and Fig. 3). Such a heterogeneity is well known phenomenon and considered as fundamental property of cellular systems [58,59] including bacteria [60]. Similarly, this heterogeneity within bacterial populations is well defined and provides a mechanism to increase range of responses to changing environmental conditions [61]. In fact, deviations of a particular parameter (e.g. in our case "MDs count per single cell", see Fig. 3) from the average in the whole population (in our case, "the averaged MDs size per all cell", see Table 1) are the basis of Darwin's theory of evolution by natural selection [62]. Therefore, our data point out to the necessity to consider population variability in cyanobacteria in future studies addressing single cells (e.g. microscopy pictures of single cell). Our data indicates that different cyanobacterial cells of the same species are not "uniform units" and cells in the population can differ significantly (see e.g. observed variability in the Fig. 2, totally green cell C1 versus "magenta cell" A4). To overcome this natural population variability, a higher number of cells (tens or hundreds) needs

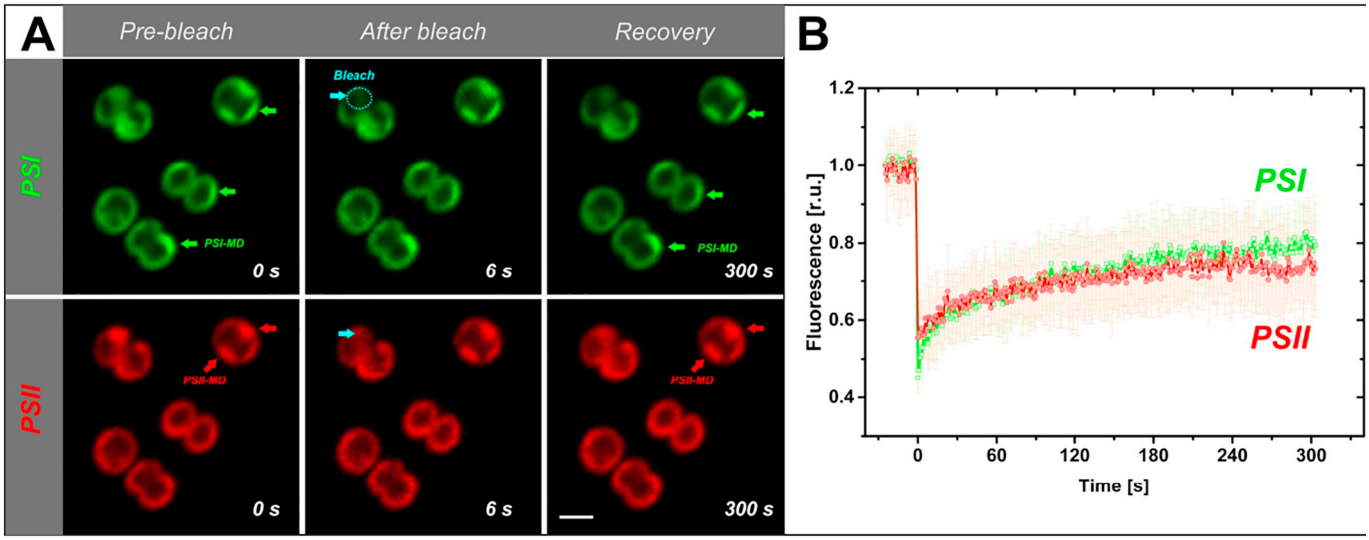

Fig. 6. Time lapse imaging of PSI and PSII fluorescence of representative FRAP image sequence of *Synechocystis* 6803 PSI-YFP cells. (**A**) FRAP image sequence cells acquired for PSI (green) and PSII (red), for pre-bleach ("0 s"), after-bleach ("6 s") and after fluorescence recovery ("300 s"). The green/red arrows show MDs with high PSI & PSII signal. Cyan arrows and circle indicates the position of the bleached area. (**B**). The averaged kinetics of PSI and PSII fluorescence in the bleached area. Data were corrected for fluorescence changes in the bleached cell and normalized to pre-bleach values (data represent mean and ± s.d. for $n = 8$). Scale bar 1.5 μm.

to be compared if we want to make robust conclusions for whole cell population.

4.1. Separation of photosystems into the distinct microdomains

Mosaic like structure of the cyanobacterial thylakoids reflects a partial separation (better say different distribution) of both photosystems. In higher plants, PSI and PSII are differently distributed between stromal/granal parts of thylakoid [22]. This heterogeneous localizations of photosystems in cyanobacteria are clearly visible in our images showing a high contrast between green and magenta MDs highly enriched in PSI and PSII, respectively (see Fig. 4 for details). The "intermediate" white/grey domain with balanced PSI, PSII and PBS (see Fig. 4 for details) could represent an area with recently described supercomplexes of all these PPCs [24].

Our data newly describes model of PSI/PSII co-localization in cyanobacteria. Up to now, there has been no conclusive model of PSI/PSII separation in the cyanobacterial thylakoids. Both, a radial heterogeneity with difference in PSI/PSII between inner and outer thylakoid layers [31,32]), and a lateral heterogeneity due to variability in PSI/PSII ratio within the single thylakoid membrane layer [33,34], have been proposed. Due to the obvious spatial restrictions of light confocal microscopy (including hyperspectral confocal fluorescence imaging [63]) the standard methods cannot resolve radial distribution of photosystems between membrane layers with the sufficient resolution. The PPCs composition of the MDs we observed thus represents an average PPCs composition of multiple thylakoid membrane layers. We can only speculate that due to the steric hindrance of PSI, preventing PSI movement into inner membrane layers, the PSI supercomplex can only be present in the most outer/inner surface thylakoid layers as described for granal thylakoids of higher plants [22]. On the other hand, the lateral heterogeneity of photosystems in cyanobacteria is more than obvious from our confocal microscopy data (see Fig. 5) and it is also in line with the previous data based on cryoimaging detection of PSI/PSII heterogeneity [34]. We do not know driving force for this spatial PSI/PSII separation but it can be some structural consequence of protein-protein and lipid-protein interactions [64], an interplay between physicochemical forces [19,20] controlled by ion compartmentation [21] or some specific protein clustering [65].

4.2. Stability of photosynthetic MDs

The limited types of hues observed in the most cells (compare green/magenta/grey hues in the Figs. 2, 5) reflects an existence of only particular combinations of PSI, PSII and PBS within thylakoids; this can be also quantified numerically by calculation of chromaticity values of thylakoid membrane (see Supplemental Fig. 8). The method can localize all thylakoid pixels into CIE1931 color space (for details see [39]). The analysis showed that 90% of thylakoid membrane pixels covered only 8.9% area of the CIE1931 color space (see Supplemental Fig. 8 and [54] for details on the method). It means that only certain combinations of fluorescence signal of PSI, PSII and PBS (i.e. their concentration ratios) are present in the thylakoid membrane mosaic. The presence of photosystems in the particular photosynthetic MD (Fig. 5) also limits their free diffusion in the membrane. The stability of photosynthetic MDs has been confirmed by FRAP and time lapse imaging (Fig. 6). This stability is closely related to the observed low mobility of PSII and PSI (Fig. 6) which is in line with previous reports (see e.g. reviews in [56,66]). Generally, mobility of photosynthetic proteins is approximately 10–100 times lower than mobility of mitochondrial OXPHOS enzymes that have a similar size as the cyanobacterial PPCs based on FRAP halftime (compare approximate 100 s with 1–5 s half time for PPCs and OXOPHOS proteins respectively, see [14,67] or reviews [56,68]). Both membranes, inner mitochondrial [69,70] and thylakoid membrane [71] are highly crowded with proteins and have similar lipid:proteins ratio around 20:80. It indicates that restricted mobility of PPCs is not solely due to a proteins crowding as proposed previously [72] but an unknown factor(s) may limit their mobility. In analogy with other biological membranes (see e.g. review of [7]), the unknown factor could be protein-protein interactions within the membrane [73], cytoskeleton corralling [74] or by lipids organization into nanodomains [2]. The photosynthetic MDs thus represent rather a stable, a skeleton-like structure with moderate dynamics during long-term (minutes) acclimations at specific conditions (e.g. "mobilization" of proteins by very intense "red" line, see [33,75,76]) or they can change faster at sub-micrometer scale [77].

The restricted mobility of photosystems has to affect redistribution of light between photosystems during the state transition process which mechanism remains still unclear in cyanobacteria (see e.g. review [78]). Indeed, the observed stability of MDs (Fig. 6) together with low abundance of the specific PSI-PBS MDs (Table 1) excludes any

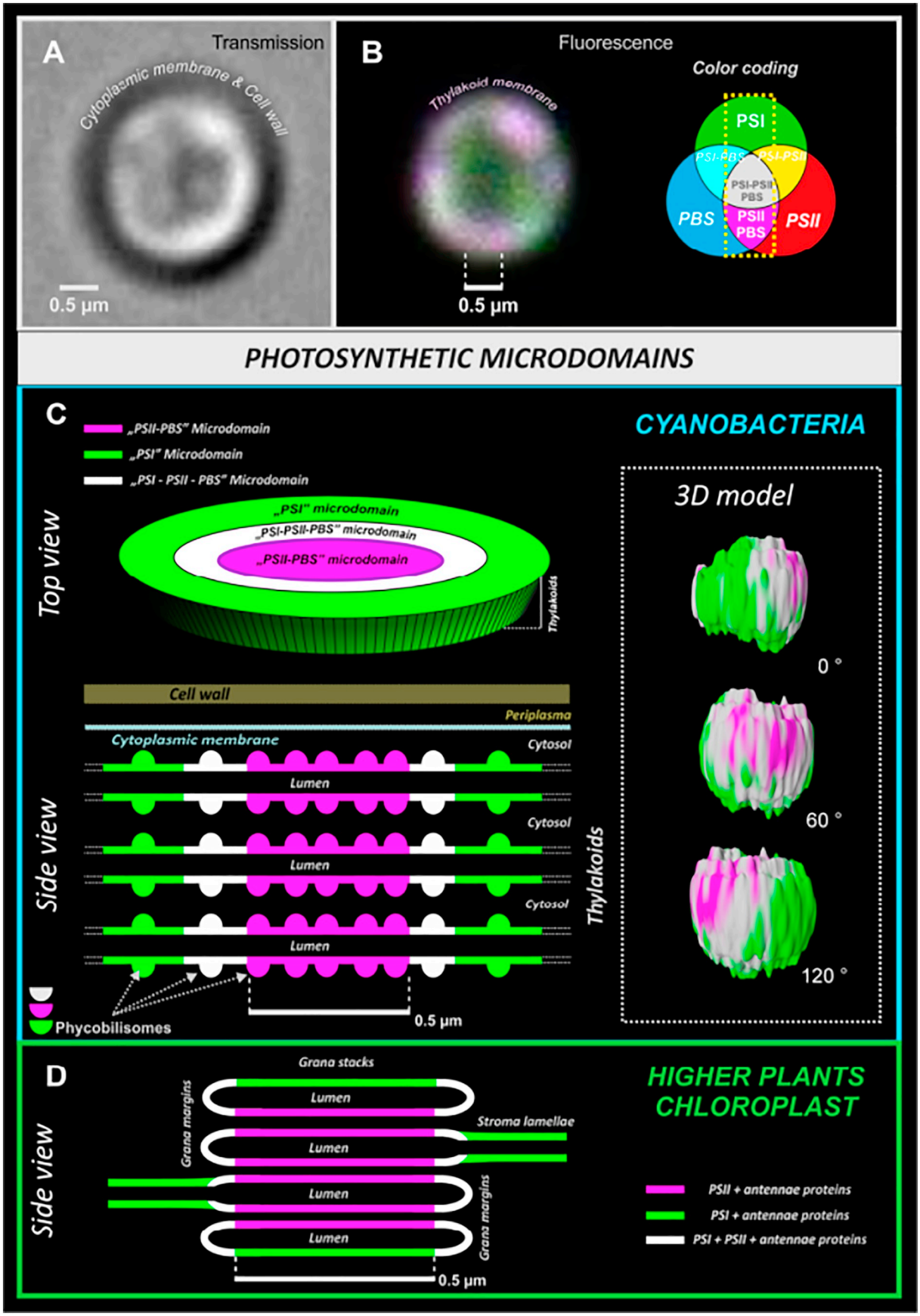

(caption on next page)

Fig. 7. Model of thylakoid membrane mosaic formed by photosynthetic microdomains (MDs) in Synechocystis 6803. The cyanobacterial model is based on our confocal image data, model of the plant thylakoid membranes was taken from Albertsson [22]. MDs are formed by photosynthetic pigment-proteins, Photosystem I (PSI – green channel), Photosystem II (PSII – red channel) and Phycobilisome (PBS – blue channel), see RGB color coding scheme.
(**A**) Bright field image of a single *Synechocystis* 6803 PSI-YFP cell with visible cytoplasmic membrane, scale bar 0.5 μm.
(**B**), Fluorescence image of the same *Synechocystis* 6803 PSI-YFP cell from the panel A. Picture shows localization of dominant photosynthetic MDs: (1) PSI MD in green; (2) PSI-PSII-PBS MD in white/grey; (3) PSII-PBS in magenta. Scale bar (0.5 μm) reflects an approximate size of single magenta MD.
(**C**) Proposed model of MDs arrangement in 3 bilayer of *Synechocystis* 6803 TMs (Top and Side view) based on experiment (Panel A) the 3D model of MDs (see Supplemental Fig. 6, Movie S6). The used colors represent dominant MDs (green, white/grey and magenta) with defined combinations of PPCs (Fig. 4); we have to note that PBS is situated on TM surface in all types of MDs. Scale bar 0.5 μm.
(**D**) Typical MDs-like organization in higher plants thylakoid that are arranged into granal and stromal membranes with margins in between. Granal thylakoid membranes contain mostly PSII with plant light-harvesting antenna proteins (resembling magenta PSII-PBS MD from cyanobacteria), stromal thylakoid membranes contains mostly PSI (resembling magenta PSII-PBS MD from cyanobacteria), and grana margins represent a mix of both (resembling white/grey PSI-PSII-PBS MD from cyanobacteria).

mechanisms requiring a long-distance movement of PPCs (including PBS) as it has been proposed previously [79,80] and also discussed for red algae [81], other photothrophs contaning PBS on membrane surface. On the other hand, this implies a mechanism of state transition relying on just a small PPCs reorganization [82] that can be further affected by membrane fluidity [83], PSI trimerization [84], phycobilisomes decoupling [85–88] or by direct excitation quenching in PSII [88].

4.3. Function of the separated stable PSII and PSI microdomains

We propose that location of PPCs (Figs. 2 and 4) in distinct MDs plays an important role in the regulation of electron and light energy transfer processes [89]. The low mobility of PPCs seems to be a prerequisite for the efficient exciton energy transfer [90] as also proposed previously for light-harvesting process in higher plant thylakoids [91,92]. In higher plants, the efficient transfer of excitations is allowed by a close interaction of either PSI or PSII with their membrane antenna proteins [93,94]) or by formation of megacomplexes of the antenna proteins with both photosystems [95,96]. On the higher mesoscopic level, reorganization of these supercomplexes into disordered/ordered arrays further affects light harvesting and lateral diffusion processes in plants (see recent reviews [97,98]). In cyanobacterial thylakoids similarly organized arrays of PPCs have also been found [36] together with active megacomplexes consisting of both photosystems with attached PBS [24]. Indeed, these nanoscale arrays of PPCs are then visible using electron transmission or atomic force microscopy (see e.g. [33,36] or reviews [99,100]). These arrays of PPCs then form the stable photosynthetic MDs visible in our 3D model of the most typical organization of cyanobacterial thylakoids, which we observed (Fig. 5).

The separation of PSII and PSI into the distinct domains can reduce excitation energy spillover from photochemically less efficient PSII towards PSI as proposed for higher plant thylakoids [101]. We need to note that the model is not valid for all observed cells due to the inevitable population heterogeneity. About 20% of the cells showed rather homogenous distribution of PPCs (see Fig. 3), in which the mechanisms responsible for MD organization of PPCs might not be working. The previously described functional nanodomains for plastoquinone diffusion between PSII and the cytochrome b_6f [102,103] are smaller in comparison to MDs, however it is plausible that they are differently distributed between MDs. A precise PSI/PSII organization is also needed for regulation of the ratio of photosynthetic cyclic/linear electron transport (see our model comparing plant/cyanobacterial thylakoids, Fig. 7) in the most typical cyanobacterial cell (see MDs variability in Fig. 3) where the PSII and PSI MDs could then represent areas with dominancy of linear and cyclic electron flow, respectively, in analogy with higher plant thylakoids [104]. The structure heterogeneity in PSII/PSI between MDs can then result in functional heterogeneity in photochemical processes that is often detected by fluorescence parameters showing domains with different rates of photoreduction [105,106].

4.4. Properties of photosynthetic microdomains in comparison to other membrane microcompartments of (cyano)bacteria and organelles

The newly described photosynthetic MDs in *Synechocystis* 6803 thylakoids have different characteristics in comparison to bacterial [107] and mitochondrial [11–13] bioenergetic MDs that are less stable and smaller. The photosynthetic MDs are much bigger (between 0.5 and 1.5 μm) in comparison to any other membrane microcompartments in cyanobacteria described before (compare 0.1–0.2 μm size of small patches of FtsH proteases [108]); bioenergetics MDs in *Gloeobacter violaceus* [37]; MDs of OXPHOS complexes [109]; nanodomains containing only PSI [35]; zones with CurT protein [110]; PratA-defined regions of proteins biogenesis (see e.g. [111] and others see review [112]). The above mentioned "*nanodomains*" were defined based on tagging of a single protein and determination of its location in a membrane region with a specialized function (e.g. biogenesis of photosystems, respiration etc.). On the contrary, the photosynthetic MDs reflect co-localization of three main pigment-protein complexes in the thylakoids - PSI, PSII and PBS – into a specific mosaic. Our three channel imaging of these PPCs was thus able to describe a system organizing these three important protein complexes. Therefore, our method allowed us to define an overall structural model of thylakoid membrane for the most typical cyanobacterial cells (Figs. 4, 5 for data and Fig. 7 for model). Our model describes thylakoid membrane as a mosaic of photosynthetic MDs; these MDs are then formed by specific ratio of PSI, PSII and PBS, their specific co-localization into MDs then affects and constrains the overall thylakoid membrane structure. It is plausible, that the other small "nanodomains" (see description above) could overlap/interact with our larger photosynthetic MDs; for instance we might attribute the center of biogenesis to a very low abundant PSII-PSI MD (Table 1) as Bečková and co-workers [113] have recently attributed supercomplexes of PSI trimers and PSII monomers to the process of photosystem biogenesis.

4.5. Comparison of cyanobacterial microdomains with structure of higher plants thylakoids

We suggest that organization of PPCs into photosynthetic MDs in *Synechocystis* thylakoids represents an evolutionary precursor of organization of higher plant thylakoids into granal/stromal parts (see Fig. 7). This is based on structural (see Fig. 7) and functional analogy as discussed in previous paragraphs. The model represents the dominating arrangement of thylakoids even within the heterogeneous population of cyanobacterial cells (see MDs variability in Fig. 3 and supplemental Table 1). Image segmentation (supplemental Fig. 3) and modelling of experimental data (supplemental Figs. 6 and 7) allowed us to re-construct a 3D model of thylakoids (Fig. 5D, supplemental Fig. 6). It shows the localization of three dominant MDs in the thylakoid membrane in the typical cyanobacterial cells (Fig. 7): a central PSII-PBS MD (in magenta) was surrounded concentrically by the PSI-PSII-PBS MD (in white/grey) and more distantly by the PSI MD shown in green (Fig. 7). This organization resembles a granal/stromal thylakoid heterogeneity

of higher plant chloroplasts as proposed long time ago [114]. Indeed, the thylakoid membrane structure in PBS-less mutants [28] resembles granal stacks similar to those in the higher plant thylakoids. Interestingly, the major magenta and green MDs have often diameter in the range of 500–1500 nm that is comparable in size with thylakoid grana of higher plants (see Figs. 3, 5 and our model in Fig. 7) ranging from 300 to 600 nm (see e.g. [115,116]. Moreover, in analogy to the cyanobacterial membranes (Fig. 4), PSII and PSI in the plant thylakoids are not strictly segregated but only unevenly distributed between granal (with more PSII) and stromal (with more PSI) thylakoids. Therefore, it is tempting to propose, that the evolutionary loss of PBS and appearance of membrane-embedded antennas in plants resulted in development of a different mechanism of PSI/PSII compartmentation (Fig. 7). Thus, during evolution the photosynthetic MDs in the unstacked thylakoids of cyanobacteria were substituted by the photosystem compartmentation based on membrane stacking (Fig. 7). This might also be connected with evolution of channels/transporters [117]) as the membrane stacking is driven by physicochemical forces [19,20] and controlled by ion compartmentation [21]. In conclusion, the described photosynthetic MDs in the cyanobacterial thylakoids can be viewed as a new example of compartmentation of cellular processes in prokaryotes (reviewed in [118]) apart from compartmentation of genetic information [119], cytoskeletal proteins [5] and bacterial sensory system [120].

5. Conclusions

We have described heterogeneous organization of all main pigment-protein complexes - PPCs (Photosystem I tagged by YFP, Photosystem II and Phycobilisomes) in the thylakoids of *Synechocystis* 6803. Our 3D confocal images depicted heterogeneous distribution of PPCs in thylakoid membranes in a form of stable MDs. These microcompartments are of sub-micrometer in sizes (~0.5–1.5 μm) and they are stable in the range of minutes. MDs are defined by particular ratios of PPCs as they contain different mix of all studied complexes – photosystems and phycobilisomes. The most prevailing MD is represented by MD with high Photosystem I content (and low PSII and PBS concentrations) that allows partial separation of Photosystems similar to stromal/granal heterogeneity of photosystems in higher plant thylakoids. Therefore, we propose that the cyanobacterial MDs might represent evolutional and functional precursor for the granal/stromal heterogeneity in higher plants thylakoids.

Supplementary data (Supplementary Figure 1 - 8; Supplementary Movie 1 - 7; Supplementary Table 1) to this article including figure captions can be found online at https://doi.org/10.1016/j.bbabio.2019.07.008.

Author contributions

R.K. and J.K. designed the research. A.S., G.S., E.K. M.T. performed the experiments; A.S. and M.T. generated PSI-YFP *Synechocystis* 6803 strain; A.S. and E.K. carried out physiological characterization of the new strain with YFP, G.S. was responsible for confocal microscopy measurements and G.K. together with G.S. then developed new methods of image processing and statistical analysis of images. R.K., A.S. and J.K. wrote the article. All authors discussed the results and commented on the manuscript.

Transparency document

The Transparency document associated with this article can be found, in online version.

Acknowledgments

The work was supported by project 16-10088S from the Czech Science Foundation and by institutional project Algatech plus (MSMT LO1416) and Algamic (CZ.1.05/2.1.00/19.0392) provided by the Czech Ministry of Education, Youth and Sport. The work od G.S. has been funded by GINOP-2.3.2-15-2016-00001 grant. The authors want to thank Jaroslav Krafl for his enthusiastic approach in taking confocal microscopy pictures of *Synechocystis* sp. 6803 cells and Eva Prachová for her long-term carring about cyanobacterial strains/mutants in the laboratory of photosynthesis.

Abbreviations

FRAP	Fluorescence after photobleaching recovery
MD	Microdomain
OXPHOS	Enzymes of oxidative phosphorylation in mitochondria
PBS	Phycobilisomes
PPCs	Pigment-Protein complexes, namely Photosystem I, Photosystem II and Phycobilisome
PSI	Photosystem I
PSII	Photosystem II
RGB	Red & Green & Blue colors system representing the 3 channel confocal imaging
σ_{PSII}	effective antenna size of photosystem II
YFP	Yellow Fluorescence Protein

References

[1] S.J. Singer, G.L. Nicolson, The fluid mosaic model of the structure of cell membranes, Science 175 (1972) 720–731.
[2] K. Simons, E. Ikonen, Functional rafts in cell membranes, Nature 387 (1997) 569–572.
[3] K. Matsumoto, H. Hara, I. Fishov, E. Mileykovskaya, V. Norris, The membrane: transertion as an organizing principle in membrane heterogeneity, Front. Microbiol. 6 (2015) 21.
[4] L. Shapiro, H.H. McAdams, R. Losick, Generating and exploiting polarity in bacteria, Science 298 (2002) 1942–1946.
[5] H. Strahl, F. Burmann, L.W. Hamoen, The actin homologue MreB organizes the bacterial cell membrane, Nat. Commun. 5 (2014).
[6] M. Sorice, V. Manganelli, P. Matarrese, A. Tinari, R. Misasi, W. Malorni, T. Garofalo, Cardiolipin-enriched raft-like microdomains are essential activating platforms for apoptotic signals on mitochondria, FEBS Lett. 583 (2009) 2447–2450.
[7] G.L. Nicolson, The fluid-mosaic model of membrane structure: still relevant to understanding the structure, function and dynamics of biological membranes after more than 40 years, Biochim. Biophys. Acta, Biomembr. 1838 (2014) 1451–1466.
[8] J. Malinsky, M. Opekarova, G. Grossmann, W. Tanner, Membrane microdomains, rafts, and detergent-resistant membranes in plants and fungi, in: S.S. Merchant (Ed.), Annual Review of Plant Biology, vol 64, Annual Reviews, Palo Alto, 2013, pp. 501–529.
[9] M. Opekarová, J. Malinsky, W. Tanner, Plants and fungi in the era of heterogeneous plasma membranes*, Plant Biol. 12 (2010) 94–98.
[10] R.H. Pan, A.D. Jones, J.P. Hu, Cardiolipin-mediated mitochondrial dynamics and stress response in Arabidopsis, Plant Cell 26 (2014) 391–409.
[11] K.M. Davies, M. Strauss, B. Daum, J.H. Kief, H.D. Osiewacz, A. Rycovska, V. Zickermann, W. Kuhlbrandt, Macromolecular organization of ATP synthase and complex I in whole mitochondria, Proc. Natl. Acad. Sci. U. S. A. 108 (2011) 14121–14126.
[12] J. Vonck, E. Schafer, Supramolecular organization of protein complexes in the mitochondrial inner membrane, Biochim. Biophys. Acta Mol. Cell Res. 1793 (2009) 117–124.
[13] D.K. Schweppe, J.D. Chavez, C.F. Lee, A. Caudal, S.E. Kruse, R. Stuppard, D.J. Marcinek, G.S. Shadel, R. Tian, J.E. Bruce, Mitochondrial protein interactome elucidated by chemical cross-linking mass spectrometry, Proc. Natl. Acad. Sci. (2017).
[14] V. Wilkens, W. Kohl, K. Busch, Restricted diffusion of OXPHOS complexes in dynamic mitochondria delays their exchange between cristae and engenders a transitory mosaic distribution, J. Cell Sci. 126 (2013) 103–116.
[15] R. Acin-Perez, J.A. Enriquez, The function of the respiratory supercomplexes: the plasticity model, Biochim. Biophys. Acta, Bioenerg. 1837 (2014) 444–450.
[16] A.V. Ruban, M.P. Johnson, Visualizing the dynamic structure of the plant photosynthetic membrane, Nat. Plants 1 (2015).
[17] M. Pribil, M. Labs, D. Leister, Structure and dynamics of thylakoids in land plants, J. Exp. Bot. 65 (2014) 1955–1972.
[18] A. Mechela, S. Schwenkert, J. Soll, A brief history of thylakoid biogenesis, Open Biol. 9 (2019) 180237.
[19] W.S. Chow, E.H. Kim, P. Horton, J.M. Anderson, Granal stacking of thylakoid membranes in higher plant chloroplasts: the physicochemical forces at work and the functional consequences that ensue, Photochem. Photobiol. Sci. 4 (2005) 1081–1090.

[20] S. Puthiyaveetil, B. van Oort, H. Kirchhoff, Surface charge dynamics in photosynthetic membranes and the structural consequences, Nat. Plants 3 (2017) 9.
[21] R. Kaňa, Govindjee, Role of ions in the regulation of light-harvesting, Front. Plant Sci. 7 (2016).
[22] P.-Å. Albertsson, A quantitative model of the domain structure of the photosynthetic membrane, Trends Plant Sci. 6 (2001) 349–354.
[23] N. Adir, Elucidation of the molecular structures of components of the phycobilisome: reconstructing a giant, Photosynth. Res. 85 (2005) 15–32.
[24] H. Liu, H. Zhang, D.M. Niedzwiedzki, M. Prado, G. He, M.L. Gross, R.E. Blankenship, Phycobilisomes supply excitations to both photosystems in a megacomplex in cyanobacteria, Science 342 (2013) 1104–1107.
[25] P.J. Keeling, The endosymbiotic origin, diversification and fate of plastids, Philos. Trans. R. Soc., B 365 (2010) 729–748.
[26] V. Zimorski, C. Ku, W.F. Martin, S.B. Gould, Endosymbiotic theory for organelle origins, Curr. Opin. Microbiol. 22 (2014) 38–48.
[27] L.N. Liu, Distribution and dynamics of electron transport complexes in cyanobacterial thylakoid membranes, Biochim. Biophys. Acta, Bioenerg. 1857 (2016) 256–265.
[28] A.M. Collins, M. Liberton, H.D.T. Jones, O.F. Garcia, H.B. Pakrasi, J.A. Timlin, Photosynthetic pigment localization and thylakoid membrane morphology are altered in Synechocystis 6803 Phycobilisome mutants, Plant Physiol. 158 (2012) 1600–1609.
[29] R. Nevo, D. Charuvi, E. Shimoni, R. Schwarz, A. Kaplan, I. Ohad, Z. Reich, Thylakoid membrane perforations and connectivity enable intracellular traffic in cyanobacteria, EMBO J. 26 (2007) 1467–1473.
[30] M. Liberton, L.E. Page, W.B. O'Dell, H. O'Neill, E. Mamontov, V.S. Urban, H.B. Pakrasi, Organization and flexibility of cyanobacterial thylakoid membranes examined by neutron scattering, J. Biol. Chem. 288 (2013) 3632–3640.
[31] W.F.J. Vermaas, J.A. Timlin, H.D.T. Jones, M.B. Sinclair, L.T. Nieman, S.W. Hamad, D.K. Melgaard, D.M. Haaland, In vivo hyperspectral confocal fluorescence imaging to determine pigment localization and distribution in cyanobacterial cells, Proc. Natl. Acad. Sci. U. S. A. 105 (2008) 4050–4055.
[32] D.M. Sherman, T.A. Troyan, L.A. Sherman, Localization of membrane-proteins in the cyanobacterium synechococcus sp pcc7942 - radial asymmetry in the photosynthetic complexes, Plant Physiol. 106 (1994) 251–262.
[33] S. Casella, F. Huang, D. Mason, G.Y. Zhao, G.N. Johnson, C.W. Mullineaux, L.N. Liu, Dissecting the native architecture and dynamics of cyanobacterial photosynthetic machinery, Mol. Plant 10 (2017) 1434–1448.
[34] G. Steinbach, F. Schubert, R. Kaňa, Cryo-imaging of photosystems and phycobilisomes in Anabaena sp. PCC 7120 cells, J. Photochem. Photobiol. B Biol. 152 (2015) 395–399 Part B.
[35] C. MacGregor-Chatwin, M. Sener, S.F.H. Barnett, A. Hitchcock, M.C. Barnhart-Dailey, K. Maghlaoui, J. Barber, J.A. Timlin, K. Schulten, C.N. Hunter, Lateral segregation of photosystem I in cyanobacterial thylakoids, Plant Cell 29 (2017) 1119–1136.
[36] I.M. Folea, P. Zhang, E.M. Aro, E.J. Boekema, Domain organization of photosystem II in membranes of the cyanobacterium Synechocystis PCC6803 investigated by electron microscopy, FEBS Lett. 582 (2008) 1749–1754.
[37] S. Rexroth, C.W. Mullineaux, D. Ellinger, E. Sendtko, M. Rogner, F. Koenig, The plasma membrane of the cyanobacterium Gloeobacter violaceus contains segregated bioenergetic domains, Plant Cell 23 (2011) 2379–2390.
[38] J. Mareš, P. Hrouzek, R. Kaňa, S. Ventura, O. Strunecký, J. Komárek, The primitive thylakoid-less cyanobacterium *Gloeobacter* is a common rock-dwelling organism, PLoS One 8 (2013) e66323.
[39] G. Konert, G. Steinbach, M. Canonico, R. Kaňa, Protein arrangement factor: a new photosynthetic parameter characterizing the organization of thylakoid membrane proteins, Physiol. Plant. 166 (2019) 264–277.
[40] A. Straskova, J. Knoppova, J. Komenda, Isolation of the cyanobacterial YFP-tagged photosystem I using GFP-Trap (R), Photosynthetica 56 (2018) 300–305.
[41] J.G.K. Williams, Construction of specific mutations in photosystem-ii photosynthetic reaction center by genetic-engineering methods in Synechocystis-6803, Methods Enzymol. 167 (1988) 766–778.
[42] M. Tichy, M. Beckova, J. Kopecna, J. Noda, R. Sobotka, J. Komenda, Strain of Synechocystis PCC 6803 with aberrant assembly of photosystem NN contains tandem duplication of a large chromosomal region, Front. Plant Sci. 7 (2016).
[43] T. Nagai, K. Ibata, E.S. Park, M. Kubota, K. Mikoshiba, A. Miyawaki, A variant of yellow fluorescent protein with fast and efficient maturation for cell-biological applications, Nat. Biotechnol. 20 (2002) 87–90.
[44] M. Dobakova, R. Sobotka, M. Tichy, J. Komenda, Psb28 protein is involved in the biogenesis of the photosystem II inner antenna CP47 (PsbB) in the cyanobacterium Synechocystis sp PCC 6803, Plant Physiol. 149 (2009) 1076–1086.
[45] I. Wittig, M. Karas, H. Schagger, High resolution clear native electrophoresis for In-gel functional assays and fluorescence studies of membrane protein complexes, Mol. Cell. Proteomics 6 (2007) 1215–1225.
[46] J. Komenda, J. Knoppova, J. Kopecna, R. Sobotka, P. Halada, J.F. Yu, J. Nickelsen, M. Boehm, P.J. Nixon, The Psb27 assembly factor binds to the CP43 complex of photosystem II in the cyanobacterium Synechocystis sp PCC 6803, Plant Physiol. 158 (2012) 476–486.
[47] J. Knoppova, R. Sobotka, M. Tichy, J.F. Yu, P. Konik, P. Halada, P.J. Nixon, J. Komenda, Discovery of a chlorophyll binding protein complex involved in the early steps of photosystem II assembly in Synechocystis, Plant Cell 26 (2014) 1200–1212.
[48] C. Klughammer, U. Schreiber, Saturation pulse method for assessment of energy conversion in PS I, PAM Appl. Notes 1 (2008) 11–14.
[49] Z.S. Kolber, O. Prasil, P.G. Falkowski, Measurements of variable chlorophyll fluorescence using fast repetition rate techniques: defining methodology and experimental protocols, Biochim. Biophys. Acta, Bioenerg. 1367 (1998) 88–106.
[50] R.J. Porra, W.A. Thompson, P.E. Kriedemann, Determination of accurate extinction coefficients and simultaneous equations for assaying chlorophylls a and b extracted with four different solvents: verification of the concentration of chlorophyll standards by atomic absorption spectroscopy, Biochim. Biophys. Acta Bioenergetics 975 (1989) 384–394.
[51] M.D. Abramoff, P.J. Magelhaes, S.J. Ram, Image processing with ImageJ, Biophoton. Int. 11 (2004) 36–42.
[52] T. Smith, J. Guild, The C.I.E. colorimetric standards and their use, Trans. Opt. Soc. 33 (1931) 73.
[53] H.S. Fairman, M.H. Brill, H. Hemmendinger, How the CIE 1931 color-matching functions were derived from Wright-Guild data, Color. Res. Appl. 22 (1997) 11–23.
[54] G. Konert, G. Steinbach, M. Canonico, R. Kaňa, Protein Arrangement (PA) factor: a new photosynthetic parameter characterizing the organization of thylakoid membrane proteins, Physiol. Plant. (2019) (accepted).
[55] R.R. Sokal, F.J. Rohlf, Biometry: The Principles and Practice of Statistics in Biological Research, Second ed., Freeman, New York, 1981.
[56] R. Kaňa, Mobility of photosynthetic proteins, Photosynth. Res. 116 (2013) 465–479.
[57] R. Agarwal, A. Matros, M. Melzer, H.P. Mock, J.K. Sainis, Heterogeneity in thylakoid membrane proteome of Synechocystis 6803, J. Proteome 73 (2010) 976–991.
[58] W.M. Elsasser, Outline of a theory of cellular heterogeneity, Proc. Natl. Acad. Sci. U. S. A. 81 (1984) 5126–5129.
[59] H. Rubin, Early origin and pervasiveness of cellular heterogeneity in some malignant transformations, Proc. Natl. Acad. Sci. U. S. A. 81 (1984) 5121–5125.
[60] K.M. Davis, R.R. Isberg, Defining heterogeneity within bacterial populations via single cell approaches, Bioessays 38 (2016) 782–790.
[61] S.J. Altschuler, L.F. Wu, Cellular heterogeneity: do differences make a difference? Cell 141 (2010) 559–563.
[62] C. Darwin, On the Origin of Species by Means of Natural Selection, or Preservation of Favoured Races in the Struggle for Life, London: John Murray, 1859, 1859.
[63] M.B. Sinclair, D.M. Haaland, J.A. Timlin, H.D.T. Jones, Hyperspectral confocal microscope, Appl. Opt. 45 (2006) 6283–6291.
[64] A. Borodich, I. Rojdestvenski, M. Cottam, Lateral heterogeneity of photosystems in thylakoid membranes studied by Brownian dynamics simulations, Biophys. J. 85 (2003) 774–789.
[65] N. Destainville, Cluster phases of membrane proteins, Phys. Rev. E 77 (2008) 5.
[66] C.W. Mullineaux, Factors controlling the mobility of photosynthetic proteins, Photochem. Photobiol. 84 (2008) 1310–1316.
[67] V.M. Sukhorukov, D. Dikov, K. Busch, V. Strecker, I. Wittig, J. Bereiter-Hahn, Determination of protein mobility in mitochondrial membranes of living cells, Biochim. Biophys. Acta, Biomembr. 1798 (2010) 2022–2032.
[68] T. Appelhans, K. Busch, Dynamic Imaging of Mitochondrial Membrane Proteins in Specific Sub-Organelle Membrane Locations, (2017).
[69] D. Ardail, J.P. Privat, M. Egretcharlier, C. Levrat, F. Lerme, P. Louisot, Mitochondrial contact sites - lipid-composition and dynamics, J. Biol. Chem. 265 (1990) 18797–18802.
[70] G. Hallermayer, W. Neupert, Lipid-composition of mitochondrial outer and inner membranes of neurospora-crassa, Hoppe Seylers Z. Physiol. Chem. 355 (1974) 279–288.
[71] H. Kirchhoff, U. Mukherjee, H.J. Galla, Molecular architecture of the thylakoid membrane: lipid diffusion space for plastoquinone, Biochemistry 41 (2002) 4872–4882.
[72] H. Kirchhoff, Molecular crowding and order in photosynthetic membranes, Trends Plant Sci. 13 (2008) 201–207.
[73] J.J. Sieber, K.I. Willig, C. Kutzner, C. Gerding-Reimers, B. Harke, G. Donnert, B. Rammner, C. Eggeling, S.W. Hell, H. Grubmuller, T. Lang, Anatomy and dynamics of a supramolecular membrane protein cluster, Science 317 (2007) 1072–1076.
[74] A. Kusumi, C. Nakada, K. Ritchie, K. Murase, K. Suzuki, H. Murakoshi, R.S. Kasai, J. Kondo, T. Fujiwara, Paradigm shift of the plasma membrane concept from the two-dimensional continuum fluid to the partitioned fluid: High-speed single-molecule tracking of membrane molecules, Annual Review of Biophysics and Biomolecular Structure, Annual Reviews, Palo Alto, 2005, pp. 351–U354.
[75] M. Sarcina, N. Bouzovitis, C.W. Mullineaux, Mobilization of photosystem II induced by intense red light in the cyanobacterium Synechococcus sp PCC7942, Plant Cell 18 (2006) 457–464.
[76] G. Steinbach, R. Kaňa, Automated microscopy: macro language controlling a confocal microscope and its external illumination – adaptation for photosynthetic organisms, Microsc. Microanal. 22 (2016) 258–263.
[77] M. Iwai, M. Yokono, A. Nakano, Visualizing structural dynamics of thylakoid membranes, Sci. Rep. 4 (2014).
[78] D. Kirilovsky, R. Kaňa, O. Prášil, B. Demmig-Adams, G. Garab, W. Adams III, Mechanisms modulating energy arriving at reaction centers in cyanobacteria, in: Govindjee (Ed.), Non-Photochemical Quenching and Energy Dissipation in Plants, Algae and Cyanobacteria, Springer Netherlands, 2014, pp. 471–501.
[79] S. Joshua, C.W. Mullineaux, Phycobilisome diffusion is required for light-state transitions in cyanobacterial, Plant Physiol. 135 (2004) 2112–2119.
[80] C.W. Mullineaux, M.J. Tobin, G.R. Jones, Mobility of photosynthetic complexes in thylakoid membranes, Nature 390 (1997) 421–424.
[81] R. Kaňa, E. Kotabová, M. Lukeš, Š. Papáček, C. Matonoha, L.-N. Liu, O. Prášil, C.W. Mullineaux, Phycobilisome mobility and its role in the regulation of light harvesting in red algae, Plant Physiol. 165 (2014) 1618–1631.
[82] M.D. McConnell, R. Koop, S. Vasil'ev, D. Bruce, Regulation of the distribution of

chlorophyll and phycobilin-absorbed excitation energy in cyanobacteria. A structure-based model for the light state transition, Plant Physiol. 130 (2002) 1201–1212.
[83] K. El Bissati, E. Delphin, N. Murata, A.L. Etienne, D. Kirilovsky, Photosystem II fluorescence quenching in the cyanobacterium Synechocystis PCC 6803: involvement of two different mechanisms, Biochim. Biophys. Acta, Bioenerg. 1457 (2000) 229–242.
[84] W.M. Schluchter, G.H. Shen, J.D. Zhao, D.A. Bryant, Characterization of psaI and psaL mutants of Synechococcus sp strain PCC 7002: a new model for state transitions in cyanobacteria, Photochem. Photobiol. 64 (1996) 53–66.
[85] R. Kaňa, O. Prášil, O. Komárek, G.C. Papageorgiou, Govindjee, spectral characteristic of fluorescence induction in a model cyanobacterium, Synechococcus sp (PCC 7942), Biochim. Biophys. Acta 1787 (2009) 1170–1178.
[86] R. Kaňa, E. Kotabová, O. Komárek, B. Šedivá, G.C. Papageorgiou, Govindjee, O. Prášil, The slow S to M fluorescence rise in cyanobacteria is due to a state 2 to state 1 transition, Biochim. Biophys. Acta Bioenergetics 1817 (2012) 1237–1247.
[87] E. Tamary, V. Kiss, R. Nevo, Z. Adam, G. Bernat, S. Rexroth, M. Rogner, Z. Reich, Structural and functional alterations of cyanobacterial phycobilisomes induced by high-light stress, Biochim. Biophys. Acta, Bioenerg. 1817 (2012) 319–327.
[88] R. Ranjbar Choubeh, E. Wientjes, P.C. Struik, D. Kirilovsky, H. van Amerongen, State transitions in the cyanobacterium Synechococcus elongatus 7942 involve reversible quenching of the photosystem II core, Biochim. Biophys. Acta Bioenergetics 1859 (2018) 1059–1066.
[89] K.B. Busch, G. Deckers-Hebestreit, G.T. Hanke, A.Y. Mulkidjanian, Dynamics of bioenergetic microcompartments, Biol. Chem. 394 (2013) 163–188.
[90] T. Mirkovic, E.E. Ostroumov, J.M. Anna, R. van Grondelle, Govindjee, G.D. Scholes, Light absorption and energy transfer in the antenna complexes of photosynthetic organisms, Chem. Rev. (2016).
[91] E. Crisafi, A. Pandit, Disentangling protein and lipid interactions that control a molecular switch in photosynthetic light harvesting, Biochim. Biophys. Acta, Biomembr. 1859 (2017) 40–47.
[92] S. Haferkamp, W. Haase, A.A. Pascal, H. van Amerongen, H. Kirchhoff, Efficient light harvesting by photosystem II requires an optimized protein packing density in grana thylakoids, J. Biol. Chem. 285 (2010) 17020–17028.
[93] S. Caffarri, R. Kouril, S. Kereiche, E.J. Boekema, R. Croce, Functional architecture of higher plant photosystem II supercomplexes, EMBO J. 28 (2009) 3052–3063.
[94] P. Galka, S. Santabarbara, T.T.H. Khuong, H. Degand, P. Morsomme, R.C. Jennings, E.J. Boekema, S. Caffarria, Functional analyses of the plant photosystem I-light-harvesting complex II supercomplex reveal that light-harvesting complex II loosely bound to photosystem ii is a very efficient antenna for photosystem I in state II, Plant Cell 24 (2012) 2963–2978.
[95] M. Rantala, M. Tikkanen, E.M. Aro, Proteomic characterization of hierarchical megacomplex formation in Arabidopsis thylakoid membrane, Plant J. 92 (2017) 951–962.
[96] M. Yokono, A. Takabayashi, S. Akimoto, A. Tanaka, A megacomplex composed of both photosystem reaction centres in higher plants, Nat. Commun. 6 (2015) 6675.
[97] H. Kirchhoff, Structure-function relationships in photosynthetic membranes: challenges and emerging fields, Plant Sci. 266 (2018) 76–82.
[98] H. Kirchhoff, Diffusion of molecules and macromolecules in thylakoid membranes, Biochim. Biophys. Acta, Bioenerg. 1837 (2014) 495–502.
[99] J.P. Dekker, E.J. Boekema, Supramolecular organization of thylakoid membrane proteins in green plants, Biochim. Biophys. Acta, Bioenerg. 1706 (2005) 12–39.
[100] R. Kouril, J.P. Dekker, E.J. Boekema, Supramolecular organization of photosystem II in green plants, Biochim. Biophys. Acta, Bioenerg. 1817 (2012) 2–12.
[101] H.W. Trissl, C. Wilhelm, Why do thylakoid membranes from higher-plants form grana stack, Trends Biochem. Sci. 18 (1993) 415–419.
[102] I.G. Tremmel, H. Kirchhoff, E. Weis, G.D. Farquhar, Dependence of plastoquinol diffusion on the shape, size, and density of integral thylakoid proteins, Biochim. Biophys. Acta, Bioenerg. 1607 (2003) 97–109.
[103] H. Kirchhoff, S. Horstmann, E. Weis, Control of the photosynthetic electron transport by PQ diffusion microdomains in thylakoids of higher plants, Biochim. Biophys. Acta Bioenergetics 1459 (2000) 148–168.
[104] J.M. Anderson, Consequences of spatial separation of photosystem-1 and photosystem-2 in thylakoid membranes of higher-plant chloroplasts, FEBS Lett. 124 (1981) 1–10.
[105] P. Joliot, J. Lavergne, D. Beal, Plastoquinone compartmentation in chloroplasts. 1. Evidence for domains with different rates of photo-reduction, Biochim. Biophys. Acta 1101 (1992) 1–12.
[106] J. Lavergne, J.P. Bouchaud, P. Joliot, Plastoquinone compartmentation in chloroplasts. 2. Theoretical aspects, Biochim. Biophys. Acta 1101 (1992) 13–22.
[107] A. Magalon, F. Alberge, Distribution and dynamics of OXPHOS complexes in the bacterial cytoplasmic membrane, Biochim. Biophys. Acta Bioenergetics 1857 (2016) 198–213.
[108] J. Sacharz, S.J. Bryan, J. Yu, N.J. Burroughs, E.M. Spence, P.J. Nixon, C.W. Mullineaux, Sub-cellular location of FtsH proteases in the cyanobacterium Synechocystis sp. PCC 6803 suggests localised PSII repair zones in the thylakoid membranes, Mol. Microbiol. 96 (2015) 448–462.
[109] L.-N. Liu, S.J. Bryan, F. Huang, J. Yu, P.J. Nixon, P.R. Rich, C.W. Mullineaux, Control of electron transport routes through redox-regulated redistribution of respiratory complexes, Proc. Natl. Acad. Sci. U. S. A. 109 (2012) 11431–11436.
[110] S. Heinz, A. Rast, L. Shao, A. Gutu, I.L. Gugel, E. Heyno, M. Labs, B. Rengstl, S. Viola, M.M. Nowaczyk, D. Leister, J. Nickelsen, Thylakoid membrane architecture in Synechocystis depends on CurT, a homolog of the Granal CURVATURE THYLAKOID1 proteins, Plant Cell 28 (2016) 2238–2260.
[111] M. Schottkowski, J. Ratke, U. Oster, M. Nowaczyk, J. Nickelsen, Pitt, a novel tetratricopeptide repeat protein involved in light-dependent chlorophyll biosynthesis and thylakoid membrane biogenesis in Synechocystis sp PCC 6803, Mol. Plant 2 (2009) 1289–1297.
[112] A. Rast, S. Heinz, J. Nickelsen, Biogenesis of thylakoid membranes, Biochim. Biophys. Acta, Bioenerg. 1847 (2015) 821–830.
[113] M. Bečková, Z. Gardian, J. Yu, P. Konik, P.J. Nixon, J. Komenda, Association of Psb28 and Psb27 proteins with PSII-PSI supercomplexes upon exposure of Synechocystis sp. PCC 6803 to high light, Mol. Plant 10 (2017) 62–72.
[114] B. Andersson, J.M. Anderson, Lateral heterogeneity in the distribution of chlorophyll-protein complexes of the thylakoid membranes of spinach-chloroplasts, Biochim. Biophys. Acta 593 (1980) 427–440.
[115] D. Kaftan, V. Brumfeld, R. Nevo, A. Scherz, Z. Reich, From chloroplasts to photosystems: in situ scanning force microscopy on intact thylakoid membranes, EMBO J. 21 (2002) 6146–6153.
[116] L. Mustardy, G. Garab, Granum revisited. A three-dimensional model - where things fall into place, Trends Plant Sci. 8 (2003) 117–122.
[117] B.E. Pfeil, B. Schoefs, C. Spetea, Function and evolution of channels and transporters in photosynthetic membranes, Cell. Mol. Life Sci. 71 (2014) 979–998.
[118] S. Govindarajan, O. Amster-Choder, Where are things inside a bacterial cell? Curr. Opin. Microbiol. 33 (2016) 83–90.
[119] P.M. Llopis, A.F. Jackson, O. Sliusarenko, I. Surovtsev, J. Heinritz, T. Emonet, C. Jacobs-Wagner, Spatial organization of the flow of genetic information in bacteria, Nature 466 (2010) 77–81.
[120] J.R. Maddock, L. Shapiro, Polar location of the chemoreceptor complex in the Escherichia-coli cell, Science 259 (1993) 1717–1723.